DE-FG22-94MT94011--11

Study of the Effects of Ambient Conditions Upon the Performance of Fan Powered, Infrared, Natural Gas Burners

Quarterly Report
January 1 - March 31, 1997

Work Performed Under Contract No.: DE-FG22-94MT94011

For
U.S. Department of Energy
Office of Fossil Energy
Federal Energy Technology Center
P.O. Box 880
Morgantown, West Virginia 26507-0880

By
Department of Engineering
Clark Atlanta University
Atlanta, Georgia 30314

Disclaimer

DISCLAIMER

Portions of this document may be illegible in electronic image products. Images are produced from the best available original document.

TABLE OF CONTENTS

page

STUDY OF THE EFFECTS OF AMBIENT CONDITIONS UPON THE PERFORMANCE OF FAN POWERED, INFRARED, NATURAL GAS BURNERS

INTRODUCTION

This quarterly technical progress report describes work performed under DOE Grant No. DE-FG22-94MT94011 during the period January 1, 1997 to March 31, 1997 which covers the last quarter of the project. The objective of this investigation is to characterize the operation of a fan powered infrared burner (IR burner) at various gas compositions and ambient conditions and develop design guidelines for appliances containing PIR burners for satisfactory performance.

The fan powered infrared burner is a technology introduced more recently in the residential and commercial markets. It is a surface combustor that elevates the temperature of the burner head to a radiant condition. A variety of metallic and ceramic materials are used for the burner heads. It has been demonstrated that infrared burners produce low CO and NOx emissions in a controlled geometric space [1]. As the environmental regulations become more stringent, infrared burners are receiving increasing interests.

The burner tested in this project is installed in a deep fat fryer. It consists of a pressurized air supply, an air/fuel mixing chamber, and a porous ceramic radiant tile, see Figure 1. Combustion takes place on the surface of the perforated ceramic tile creating a radiant heat source. One main reason for the present interest in this type of burner is its low NOx emissions. This is attributed to the fact that a large proportion of the heat of combustion is given out as radiation from the burner surface. This results in relatively low gas temperature in the combustion zone compared to that of a conventional free-flame burner. Applications of radiant burners include boilers, air heaters, deep fat fryers, process heaters, and immersion heaters.

The performance of natural gas-fired heating and cooking equipment is strongly dependent on ambient conditions and natural gas composition. In the United States, ambient temperature, pressure, and relative humidity vary significantly by location and season. Also, natural gas compositions supplied by local gas distribution companies exhibit seasonal and regional variations. These variations can cause reliability and performance problems in gas-fired equipment. In service, IR burners have had reliability and performance problems, especially when exposed to various gas compositions, operating altitudes, and other ambient conditions like temperature and humidity. These parameters also affect the composition of the gaseous emissions from these burners. Burning characteristics will differ in important respects, one of the most being speed of

flame propagation. It is the responsibility of the manufacturers to design appliances capable of performing more satisfactorily under reasonably wide variations in gas composition while retaining desirable efficiencies and operation.

There have been very limited studies to investigate the effects of gas composition upon the performance of radiant burner. Due to the lack of data and fundamental understandings, the IR burner product development in the industry is empirical in nature, and is conducted with one gas composition. This project characterizes the operation of IR burner at various gas compositions and ambient conditions and develops a baseline theoretical analysis to predict the behavior of these burners to the change in fuel compositions.

PROGRESS TO DATE

This project consists of both experimental research and numerical analysis. To conduct the experiments, an experimental setup has been developed and installed in the Combustion Laboratory at Clark Atlanta University, see Figure 2. This setup consists of a commercial deep fat fryer that has been modified to allow in-situ radiation measurements on the surface of the infrared burner via a view port installed on the side wall of the oil vat. Proper instrumentation including fuel/air flow rate measurement through mass flow controllers, exhaust gas emission measurement, and radiation measurement has been developed. Since accurate IR radiation measurement plays a critical role for the success of this project, various instrumentation to measure the radiant output from the infrared burner have been evaluated. In the developed experimental setup, an FTIR, System 2000 from Perkin Elmer (Perkin-Elmer Co., Norwalk, CT) is used for in-situ measurements of the radiant output from the surface of the burner. This spectroscopy system consists of a 15798.01 cm^{-1} reference laser, an external source and an internal (temperature stabilized wire coil) source options, a 12.50 mm Jacquinot-stop aperture with the resolution of 6.48 cm^{-1}, an interferometer with a beamsplitter of 6500 - 450 cm^{-1}, and an air-cooled triglycine sulfate detector (TGS, 15600 - 200 cm^{-1}). The TGS detector has a better background contribution compared to other kinds of detectors, which is important for the wide-band radiation measurement. Perkin-Elmer Spectrum for Windows version 1.0 software was used for spectral manipulation. All radiation measurements were conducted by using the burner as the external source. The effective aperture window size for the external source and the distance between the external source and instrumental interferometer were precisely controlled in the same conditions for all of the measurements. For reducing the fluctuation of test conditions, 4 scans were added and averaged for each spectra with a nominal resolution of 8 cm^{-1} in the range of 6500 - 450 cm^{-1}. Before the radiation measurements, the instrument was usually warmed up for

more than two hours and, bu design, it automatically tuned up (aligned) for the maximum sensitivity. Then a background spectrum from room-temperature-air was taken. The radiation-measurement spectral manipulation such as baseline correction and subtraction were made from the background measurement. Since the radiant signals were very strong, (the measurement noises were relatively small), the spectra were used for the total radiant energy calculation without further noise reduction and smoothing. The FTIR spectroscopy was calibrated for the radiant energy calculation by using a Graseby Infrared 564 blackbody (Graseby Co. Orlando, Florida).

An exhaust analysis system, consisting of six commercial Horiba gas analyzers (Horiba Instruments Inc., Irvine, CA) and a lab-made sampling manifold, was used to collect exhaust gases for CO, CO_2, O_2, NOx and total unburned hydrocarbon (UHC) analyses. The gas analyzer was calibrated with gases of known composition. The exhaust gas sample was continuously taken through a ¼-inch stainless steel tube from the chimney of the burner. The tip of the sampling tube was placed in the middle of the burner chimney (about 5 inch deep from the top of the chimney). A gas pump was connected to the sampling tube to convert the traditional vacuum-gas-sampling system for the gas analyzer to a positive-pressure-gas-sampling system, which significantly reduced the air diffusion into the sample gas and increased the measurement reliability. And during the emission measurement, the view port for the IR measurement were completely sealed to avoid air leakage into the combustion zone. Three measurements were made for each test condition and their average was used for the final calculation and discussion. The relative standard deviations of three measurements for all the experiments were less than 1%.

Experiments have been conducted for an extensive test matrix of fuel gas mixtures that represent the complete range of gas compositions usually encountered in the United States. Methane is used as the baseline fuel. Mixtures of methane/propane, methane/hydrogen, and methane/nitrogen are tested to study the effect of fuel mixtures on the performance of the radiant burners. The performance of the burner are investigated in terms of its radiant efficiency (ratio of radiative flux generated by the burner to the total energy input by fuel) and gaseous emissions at various gas compositions and air/fuel ratios.

Radiation Measurement

The infrared spectrum from a commercial deep fat frier, shown in Fig. 3, covers the IR range from 6500 to 450 cm^{-1} and concentrates its spectral intensity in the 4000 to

500 cm^{-1} wavenumber range with strong H_2O absorbances at 2000 - 1400 and 3700 - 3650 cm^{-1}, and CO_2 absorbances at about 2350, 2330 and 667 cm^{-1} [1-3], respectively. The measured spectrum is used to calculate the total radiant energy from the burner, as shown in Fig. 4, since the radiant energy is proportional to the integration of the measured spectrum within the wavenumber range.

During this study, it was found that measurements made at different times for the same experimental conditions produced different spectra due to variations of the analytical instrument. This, without correction, would lead to a great deviation and unreliable results. In this regard, a new FTIR analytical method has been developed which will be reported later. Using this method, the measurement variances have been eliminated, and consistent and reliable results have been obtained.

Blackbody Calibration

To quantify the radiant energy out through the measured spectrum, a blackbody has been used to calibrate the FTIR. A blackbody absorbs all of the radiant energy emitted to it. Moreover, the radiant energy emitted by a blackbody depends on its temperature alone. Therefore, the radiant energy emitted from the blackbody can be controlled precisely by simply controlling its temperature.

A Graseby Infrared blackbody was used for the calibration, and its infrared spectrum in Fig. 5 was shown to be very similar to that from a gas burner (see Fig. 3), which also covers the infrared range of 6500 - 450 cm^{-1}, and has the strong intensity distribution between 4000 and 500 cm^{-1}. When plotting the two spectra together, they are well overlapped with each other, except for the CO_2 absorbance peak, as shown in Fig. 6. This is because the blackbody was heated by electricity. The CO_2 absorbance from the blackbody's spectrum was caused by the atmospheric CO_2, which was only about 0.04% by volume. On the other hand, the gas burner was heated by burning fuel in air, where up to 12% of CO_2 could be present. Calibration has been carried out in which the blackbody's temperature was increased step by step and the spectrum at each temperature was measured and integrated to obtain the total area under the spectrum. This integrated magnitudes of the blackbody spectra from 6500 to 450 cm^{-1} were then compared with the known total radiant energy output from the blackbody, which was calculated from its

operating temperature. As expected the integrated area proportionally increased as the blackbody's temperature increased (see Fig. 7). A fourth-order-polynomial equation between the integrated area and the blackbody's temperature were obtained through regression:

$$a = 2418.7 - 38.51\,T + 0.2075\,T^2 - 2.825 \times 10^{-4}\,T^3 + 1.583 \times 10^{-7}\,T^4 \quad (1)$$

where a is the integrated area of the infrared spectra from 6500 to 450 cm^{-1}, T is the temperature in °C, and the regression coefficient is $R^2 = 0.9984$.

On the other hand, the radiant energy (or emissive power) $E_{b,\lambda}(\lambda,T)$ of a blackbody at a given wavelength λ and absolute temperature T is given by Planck's law [6] as

$$E_{b,\lambda}(\lambda,T) = C_1 / \{\lambda^5 (e^{C2/\lambda t} - 1)\} \quad (2)$$

The total radiant energy $E_b(T)$ of the blackbody is the radiation emitted by it at all wavelengths. Mathematically, it is expressed as the Stefan-Boltzmann law [7]:

$$E_b(T) = \int_0^\infty E_{b,\lambda}(\lambda,T)\, d\lambda = \delta \bullet T^4 \quad (3)$$

Where, δ is the Stefan-Boltzmann constant given by

$$\delta = (\pi/C_2)^4\, C_1/15 \quad (4)$$

where $C_1 = 3.743 \times 10^8$ W-$\mu m^4/m^2$, and $C_2 = 1.4387 \times 10^4$ μm K. By combining Eqs. 3 and 4, we have

$$E_b(T) = 5.685 \times 10^{-8} \bullet T^4 \quad (5)$$

where $E_b(T)$ is in W/m^2 and T is in K. Eq. 5 is the result of the Stefan-Boltzmann law integrated for wavelength from 0 to ∞ (or wavenumber from ∞ to 0). Since the result in Fig. 5 shows that most of the radiant energy from the infrared burner is located in the range of 4000 to 500 cm^{-1}, it is reasonable to assume the spectrum from this wavenumber range can effectively represent the total radiant energy with negligible error. Therefore, by using Eq. 5, the total radiant energy, $E_b(T)$, from the blackbody is plotted against its temperature in Fig. 6, where the units for the E_b and T have been converted into W/cm^2

and °C, respectively. Since both Eqs. 1 and 5 are fourth order, the curve in Fig. 8 is similar to that in Fig. 7.

By combining the data in Fig. 7 and 8, the total radiation energy, $E_b(T)$, is plotted against the integrated infrared energy magnitude in Fig. 9, which shows a very-well-fitted straight line with regression equation as

$$E_b(T) = -0.06391 + 2.975 \times 10^{-4}\, a \qquad (6)$$

where a is the IR magnitude integrated from 6500 to 450 cm^{-1}, the regression coefficient is $R^2 = 0.9921$.

Radiant Energy Measurement

All the radiant energies were calculated from the measured and corrected infrared data by using Eq. 6. The radiant efficiency was defined as the ratio of the calculated radiant energy to the combustion enthalpy (energy) of the input fuels.

Fig. 10 shows the IR radiant energies measured at different equivalence ratio Φ, which is defined as the ratio of the actual fuel-air ratio to the theoretical fuel-air ratio. It can be seen that in the fuel-lean combustion region as the equivalence ratio increased from 0.55 to 0.95, the radiant efficiency increased. At $\Phi = 1$, where the stoichiometric fuel-air ratio for combustion was reached, the radiant efficiency reached its maximum, ~31.4%. After that point, the combustion took place in the fuel-rich combustion region. As Φ was further increased, the radiant efficiency decreased, due to the reduced burner surface temperature due to heating the excess air. Further, Fig. 10 shows that the maximum radiant efficiency of the combustion occurred in a range where $0.95 < \Phi < 1$. This may be due to the uncertainties of air flow rate measurement caused by air leaking from opened-to-the-atmosphere view port for the radiation measurement. In order to determine the effect caused by the air leakage, a glass window was used to seal the open view port and the measurement was made by passing the infrared radiation through the glass window. Since glass had strong absorbances in some IR bands, the measured absolute spectral magnitudes were distorted and much smaller in magnitude. However, these measurement showed that radiant efficiency reached its maximum exactly at $\Phi = 1$, see Fig. 10.

Effect of Nitrogen on Radiant Efficiency

Fig. 11 shows that as nitrogen was added to the methane-air mixture before combustion the radiant efficiency was decreased and the maximum efficiency region was shifted to the fuel-rich range. This may be caused by the gas dilution. Since nitrogen is a non-combustible gas, it absorbs the energy when it is added to the combustion. As 2.4% and 7% of nitrogen (based on the amount of methane) were added to the methane-air mixture, the radiant efficiency of combustion were decreased by about 1% and 3%, respectively. In the fuel-lean combustion region, since the relative amount of the fuel was less, the nitrogen-dilution effects were greater, which resulted in the maximum efficiency region shifted to the fuel-rich combustion region.

Effect of Propane on Radiant Efficiency

The results in Fig. 12 indicate that the addition of propane to the methane did not affect much on the radiant efficiency of the combustion, at least in the fuel-lean combustion region. This is because propane and methane have quite similar physical and chemical property. Both propane and methane are straight chain saturated hydrocarbons at the gaseous state in the ambient temperature and pressure. They also produce the same combustion products, CO_2 and water, as shown in Eqs. 7 and 8.

$$\mathbf{CH_4 + 2\ O_2 = CO_2 + 2\ H_2O} \qquad (7)$$

$$\mathbf{C_3H_8 + 5\ O_2 = 3\ CO_2 + 4\ H_2O} \qquad (8)$$

When completely combusted in the air, the exhaust produced from one mole methane consists of $N_2 = 2 \times 79/21 = 7.52$ moles, $CO_2 = 1$ mole, and $H_2O = 2$ moles. The heat capacities of N_2, CO_2 and H_2O are 29.1, 37.1. and 33.6 J/mole•K, respectively [8]. So the total exhaust gas heat capacity from one mole methane combustion is $7.52 \times 29.1 + 1 \times 37.1 + 2 \times 33.6 = 323.2$ J/K, (mole × J/mole•K = J/K). The total exhaust gas heat capacity from one mole propane combustion is $(5\times79/21)\times29.1 + 3\times37.1 + 4\times33.6 = 793.1$ J/K. The combustion enthalpies for Eqs. 7 and 8 are 890.8 and 2219 kJ/mole, respectively [8]. If only the exhaust gas is heated and the changes of the heat capacities with temperature are omitted, the maximum exhaust gas temperature increases by combusting one mole methane and propane are $890.8\times1000/323.2 = 2756$ and

2219×1000/793.1 = 2798 K/mole, respectively This indicates, thermodynamically, the substitution of methane with propane will not noticeably affect the unit combustion heat. It should be mentioned that if burned with pure oxygen, propane will produce a higher molar combustion heat because its exhaust gas is reduced by 5 × 79/21 = 18.8 moles of nitrogen. For methane, the total number of moles of exhaust gas will be reduce by only 2 × 79/21 = 7.5 moles. On the other hand, for the saturated straight-chain hydrocarbons as the number of carbon increases, its stability increases. That is, kinetically its ignition (combustion) becomes more difficult. Especially in the situation where the thermodynamic force is weak, such as insufficiency of reactant (oxygen), the kinetic effect becomes dominant that some of propane molecules could not be combusted fast enough in the combustion region near the surface of the ceramic tile of the burner. Most of these unburned hydrocarbons were transported with the emission gases from the burner top to the chimney and eventually completely consumed there. This has been observed in the study, and it is believed that the unburned propane leaded to the decreased radiant efficiency.

Effect of Hydrogen on Radiant Efficiency

Fig. 13 illustrates that the hydrogen addition to the methane-air combustion increased the radiant efficiency. Hydrogen was combusted as follow,

$$H_2 + ½ O_2 = H_2O \qquad (9)$$

The combustion enthalpy for Eq. 9 is 241.8 kJ/mole [8]. Burning one mole of hydrogen in air, the maximum temperature increase is 241.8×1000/(0.5 × 79/21 × 29.1 + 1 × 33.6) = 2737 K/mole hydrogen. This is quite close to that from the combustion of methane. Therefore, the radiant efficiency should be sirnilar to that of methane. However, probably like the propane combustion, the kinetic factor plays a critical role again. Hydrogen molecules have lower ignition activation energy than methane. They can be more quickly ignited and more thoroughly combusted in the combustion region near the surface of the burner, which leads to the higher radiant efficiency.

Emission Measurement

The compositions of the combustion exhaust gases were more sensitive to the changes of the combustion conditions.

According to Eq. 7, CO_2 is the one of the final combustion products of methane. In a given condition, the CO_2 concentration was found to be proportional to the combustion efficiency, see Fig. 14. Fig. 14 shows that in the fuel-lean combustion region, as the equivalence ratios Φ increased from 0.5 to 1, the concentrations of the CO_2 in the exhaust increased from 7.5% to 10%. At Φ = ~1, where the stoichiometric fuel-air ratio for combustion was reached, the concentration of CO_2 arrived at its maximum, 10.7%. Theoretically, when a mole of CH_4 is completely combusted in air it will consume 2 moles of oxygen and produce one mole of CO_2 and 2 moles of water plus $2 \times 79/21$ moles of nitrogen. If the produced water vapor is not condensed, at the stoichiometric fuel-air ratio (Φ = 1), the CO_2 concentration in the combustion exhaust should be $1/(1+2+2\times79/21) = 9.5\%$. On the other hand, if the water vapor is completely condensed, the CO_2 concentration should be $1/(1+2\times 79/21) = 11.7\%$. It is believed that some of the water vapor still existed in the sampling system. Therefore, the 10.7% of the CO_2 concentration at the stoichiometric combustion may indicate complete combustion of methane in the air. This was confirmed by the analysis of the unburned hydrocarbons, see later.

In the fuel-lean combustion region, where the air was in excess, the concentration of O_2 was shown to proportionally decrease as the equivalence ratio increased until to about Φ = 1, where the O_2 concentration reached its lowest point, ~ 0.2% (see Fig. 15). After that, as the equivalence ratio further increased, the O_2 concentration did not effectively change but kept at about 0.2%.

In the case of the oxygen deficiency, occured in the fuel-rich combustion, the CO concentration becomes significant. According to following equilibrium between CO_2 and CO,

$$\mathbf{CO_2 = CO + \tfrac{1}{2} O_2} \quad \mathbf{(10)}$$

the concentration of CO is heavily dependent on the O_2 concentration. Since the equilibrium constant is very small, $K = 8.2\times10^{-46}$ at 298 K and 1.7×10^{-8} at 1200 K, respectively, the CO concentration will be very small if there is enough oxygen existed. The experimental results in Fig. 15 indicate that in the fuel-lean combustion region,

because of the excess air, the CO concentration was very slowly increased from 240 to 320 ppm as Φ was increased from 0.75 to 1. As soon as the combustion was moved into the fuel-rich region, the CO concentration immediately jumped to 4300 ppm at Φ = 1.02. Since the instrumental measurement limitation for CO is 5000 ppm, the higher CO concentration could not be determined.

Similar to the concentration of CO, the unburned hydrocarbon (UHC) is also an function of the O_2 concentration. As mentioned previously, the hydrocarbons that were not burned near the surface of the burner would be consumed further downstream. As a result, the measured unburned composition near the exit of the burner was quite close to equilibrium state. In the fuel-lean combustion region, the concentrations of the total unburned hydrocarbons were increased slowly from 100 to 300 ppm as Φ increased from 0.6 to 1, as shown in Fig. 16.

NOx is mainly the mixture of NO and NO_2 and they are formed in flame by following reactions [9],

$$\mathbf{N_2 + O_2 = 2\,NO} \qquad \mathbf{(11)}$$

$$\mathbf{NO + \tfrac{1}{2}\,O_2 = NO_2} \qquad \mathbf{(12)}$$

Because both of Eqs. 11 and 12 are reversible reactions, NOx concentration should be the function of oxygen concentration. However, Fig. 17 shows that, similar to CO_2, the NOx concentration was heavily dependent on the equivalence ratio, and had a maximum value at close to Φ = ~1, ~7.5 ppm, except for that the NOx curve reached its maximum value earlier than CO_2 did. This phenomena may be caused by the kinetic factors. Since the formation rate of NOx was found to be mainly controlled by the kinetic factors [9], the concentrations of NOx in the exhaust gases are mainly the function of combustion temperature. In the region of Φ = ~ 1, the burner reached its highest temperature, and as the Φ went away from stoichiometric ratio to either side, the burner's temperature proportionally went down. As a result, the NOx concentration curve appeared to have a similar shape as CO_2. The divergence between NOx and CO_2 curves means that the stoichiometric combustion may not always produce the maximum temperature for radiant burners, because it also depends on other factors such as the flame shape. The shift of the

NOx curves to fuel-rich region further indicated that some of the hydrocarbons may not be burned near the tile surface of the radiant burner. This fuel-rich shift for the NOx curve was also found from the combustion of an auto engine [9]. Because of its relatively uniform temperature distribution, the IR porous burner did not produce very high temperature spots. Compared with the traditional types of burners, the NOx produced from this radiant burner was lower [10]. This exemplifies one of the advantages of IR radiant burners.

Effect of Nitrogen on Emission Gases

Fig. 18 shows that as the addition of nitrogen increased the CO_2 concentration was decreased slightly but the maximum CO_2 concentration position relative to equivalence ratio did not change. This is because nitrogen is non-combustible gas, when it was added to the methane-air combustion gas, it only worked as a dilutent. As the dilution increased, the concentration of the CO_2 decreased. The CO_2 concentration decrease also caused the equilibrium of Eq. 10 moved to the left-hand side, that is, the decrease of the CO concentration. Correspondingly, the CO formation curve shifted to the lower-O_2-concentration direction, that is, the fuel-lean combustion direction, as shown in Fig. 19. Further more, the nitrogen addition (dilution) reduced the combustion temperature, which should decrease the combustion rate. This should result in more unburned hydrocarbons. Most of these unburned hydrocarbons were believed to be burned along the way to the chimney. Therefore, the total unburned hydrocarbon results as shown in Fig. 20 appeared almost the same as that without nitrogen addition. Fig. 21 indicates some decrease of the NOx concentration after nitrogen addition, which was probably caused by the decrease of the combustion temperature.

Effect of Propane on Emission Gases

Fig. 22 shows that the CO_2 concentration curves shifted to the fuel-lean region as propane was added to the methane-air mixture. This confirmed the results and discussions from the radiation measurements: because of propane's higher kinetic inertness, stronger thermodynamic condition, such as reactant oxygen, was needed for its reaction (combustion). Fig. 22 also indicates that the CO_2 maximum concentration for 18% propane addition was increased by about 0.2% compared to that of no propane addition.

According to Eqs. 7 and 8, the CO_2 concentration produced for complete propane combustion is $3/(5\times79/21 + 3 + 4) = 11.6\%$ compared to 9.5% for the complete methane combustion. For the same kinetic reason, Fig. 23 illustrates that the CO curves also shifted to the fuel lean region. Similar to the nitrogen addition, most of the unburned-hydrocarbons were burned on the way to the chimney, so the total unburned hydrocarbon results in Fig. 24 did not show any significant change. Although, as discussed previously, propane did not increase the molar combustion heat, its addition did increase the total combustion heat. This resulted in the higher combustion temperature and greater NOx formation, as shown in Fig. 25.

Effect of Hydrogen on Emission Gases

Fig. 26 shows that as hydrogen was added to the methane-air mixture the CO_2 concentrations in the combustion emission gas went down. This is due to that there is no CO_2 formation from the H_2 combustion (see Eq. 9). The combustion products (H_2O and N_2) from the H_2 combustion worked in similar way as nitrogen. They diluted the concentration of the CO_2 produced from methane's combustion, which leaded to the decrease of CO_2 concentration in the exhaust. Same as the nitrogen addition, as the CO_2 concentration went down, the movement of the equilibrium of Eq. 10 resulted in the shift of the CO curve toward in the fuel-lean combustion, as shown in Fig. 27. Fig. 28 illustrates that, similar as the situations of the propane/nitrogen addition, the hydrogen addition did not change the total unburned hydrocarbon concentrations, which were still only dependent on the equivalence ratios. However, since hydrogen has a lower molar combustion enthalpy than methane does, the results in Fig. 29 indicate that the NOx formation went down a litter due to reduced temperature when hydrogen was added.

CONCLUSIONS

- Fourier transform infrared spectroscopy is a simple, fast, reliable and nondestructive analytical method. By using the method developed in Clark Atlanta University, consistent and reliable infrared spectral results can be obtained. An accurate radiant energy can be calculated from these infrared spectra by using a blackbody as the calibration standards.

- By means of the specially-designed-&-lab-made sampling inlet and the Horiba gas analyzers, the compositions of CO_2, CO, UCH, NOx and O_2 etc. from the combustion exhaust gases have been on-line accurately analyzed.
- The commercial natural gas IR burner performed differently in the different conditions. For the methane-air combustion, at the equivalence ratio $\Phi = 1$, the IR burner produced its maximum radiation efficiency, ~31.4%, and the concentration of CO_2 reached its maximum value, ~ 10.7%. In the fuel-lean region, the O_2 concentration in the emission gas decreased proportionally as Φ increased, but the concentrations of CO and UHC were kept in a couple of hundred ppm ranges. In the fuel-rich region, the O_2 concentration was kept as a constant, ~ 0.2%, but the CO and UHC concentrations were quickly jumped to thousands ppm or more as Φ further increased. The NOx formation was mainly dependent on the combustion temperature, and reached its maximum, ~8 ppm, at $\Phi = \sim 1$. Because of the uniform temperature distribution, the IR burner produced lower NOx than traditional gas burners.
- Nitrogen is a non-combustible gas. It worked only as dilutent for the combustion, reducing the radiant efficiency. Propane has a higher molar combustion enthalpy. It produced a higher combustion temperature and NOx, while maintaining similar radiant efficiency. Hydrogen has a lower combustion activation energy. It enhanced the radiant efficiency, and did not significantly affect the production of NOx, CO_2 and CO.

ACKNOWLEDGMENTS

This work was supported by US Department of Energy, through Contract No. DE-FG22-94MT94011 and natural gas industry. AGA Research is our industrial partner.

REFERENCE

1. Taylor, J.H.; Benedict, W.S. and Strong, J.; *J Chem. Phys.*, 20, 1952, p. 1884.
2. Nakamoto, K.; *Infrared Spectra of Inorganic and Coordination Compounds*, 2ed ed., John Wiley & Sons Inc., New York, 1970, p. 17-18, 83.
3. *CRC Handbook of Basic Tables for Chemical Analysis*, p. 519.

4. "A Method for Measuring the Radiant Energy by an Internal-Standardized Fourier Transform Infrared Spectroscopy," US Patent applied.
5. Dird, R.B.; Stewart, W.E. and Lightfoot, E.N.; *Transport Phenomena*, John Wiley & Sons Inc., New York, 1960, p. 427-437.
6. Plank, M.; *Vorlesungen uber die Theorie der Warmestrahlung*, 5th ed., Barth Leipzig, 1923.
7. Dorf, R.C., ed.; *The Engineering Handbook*, CRC Press Inc., Boca Raton, 1996, p.518-520.
8. Lide, D.R., ed.; *CRC Handbook of Chemistry and Physics*, 73rd ed., CRC Press Inc., Boca Raton, 1992, p.10-300 - 10-301.
9. Nevers, N. de; *AIR POLLUTION CONTROL ENGINEERING*, McGraw-Hill Inc., New York, 1995, p.378-393, 416.
10. Yeboah, Y.D.; "Turbulent Premixed Methane-Air Combustion: Emissions, Characteristics and Modeling," *An Technical Report to NASA*, Clark Atlanta University, July, 1997.

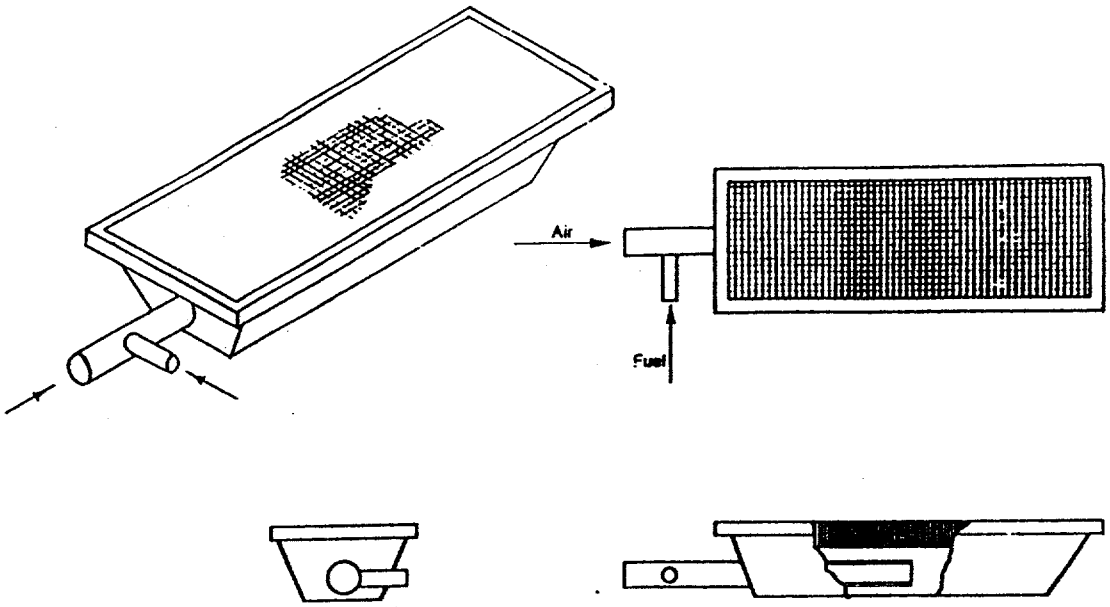

Figure 1 A schematic of the infrared burner.

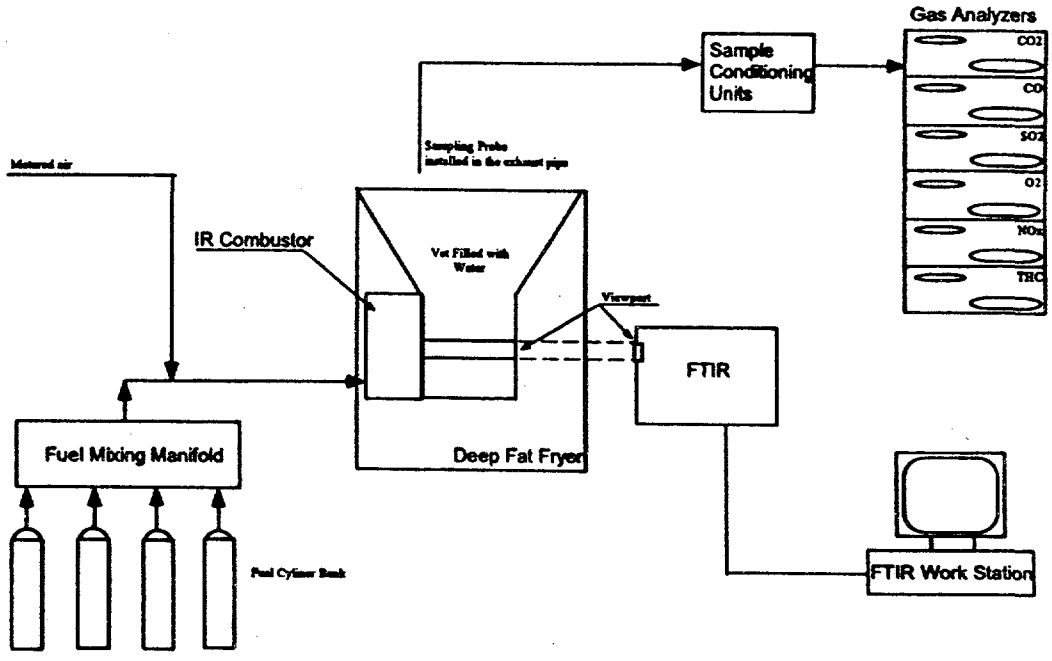

Figure 2 A schematic of the experimental setup.

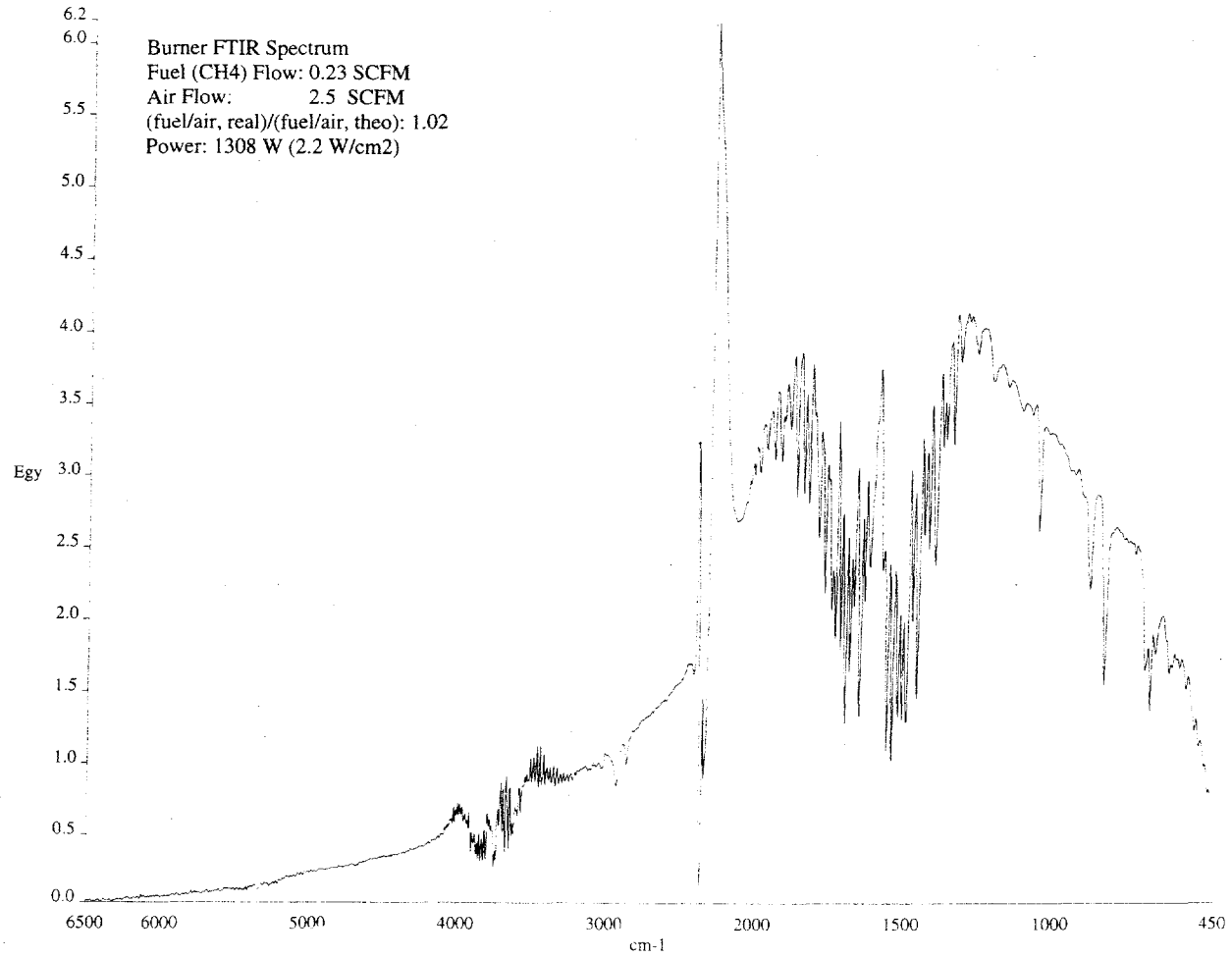

Fig. 3 FTIR spectrum of the infrared burner.

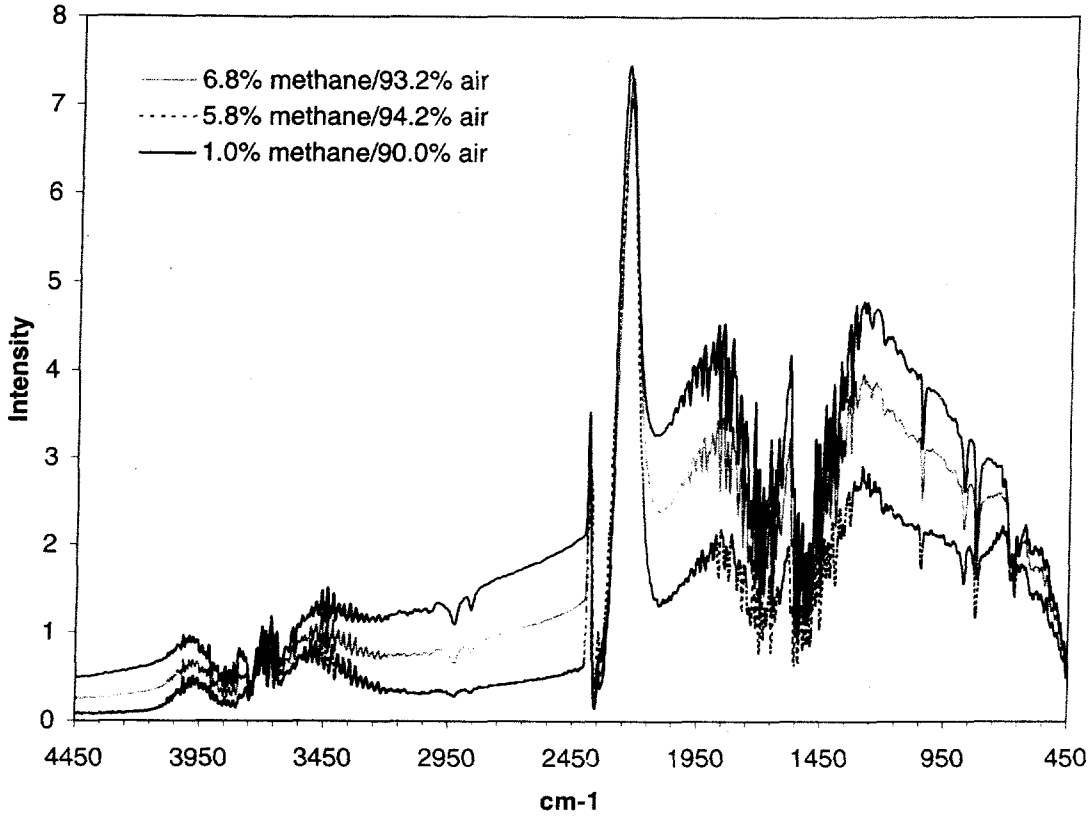

Fig. 4 FTIR spectrum of the infrared burner at different methane/air ratios

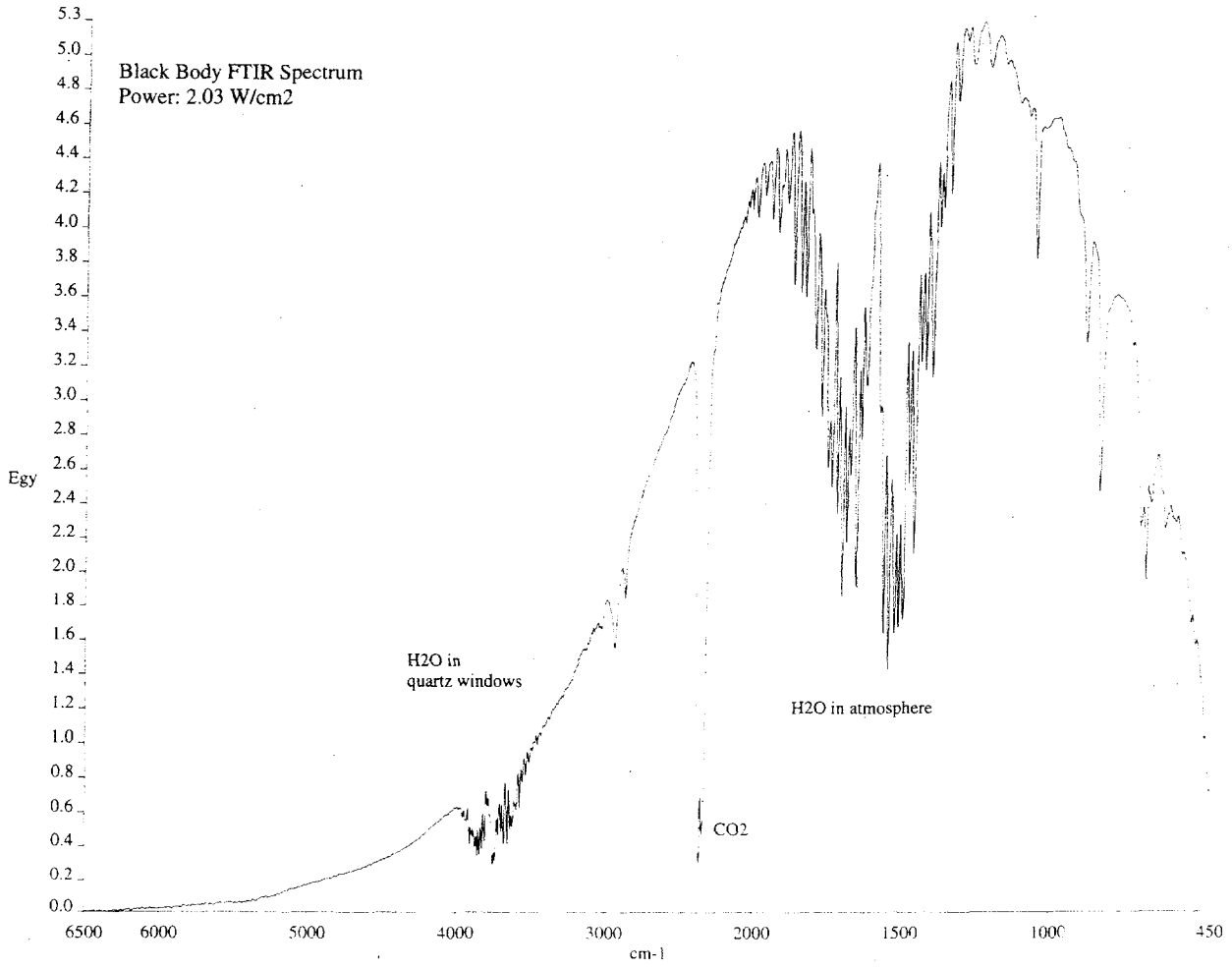

Fig. 5 FTIR spectrum of the black body.

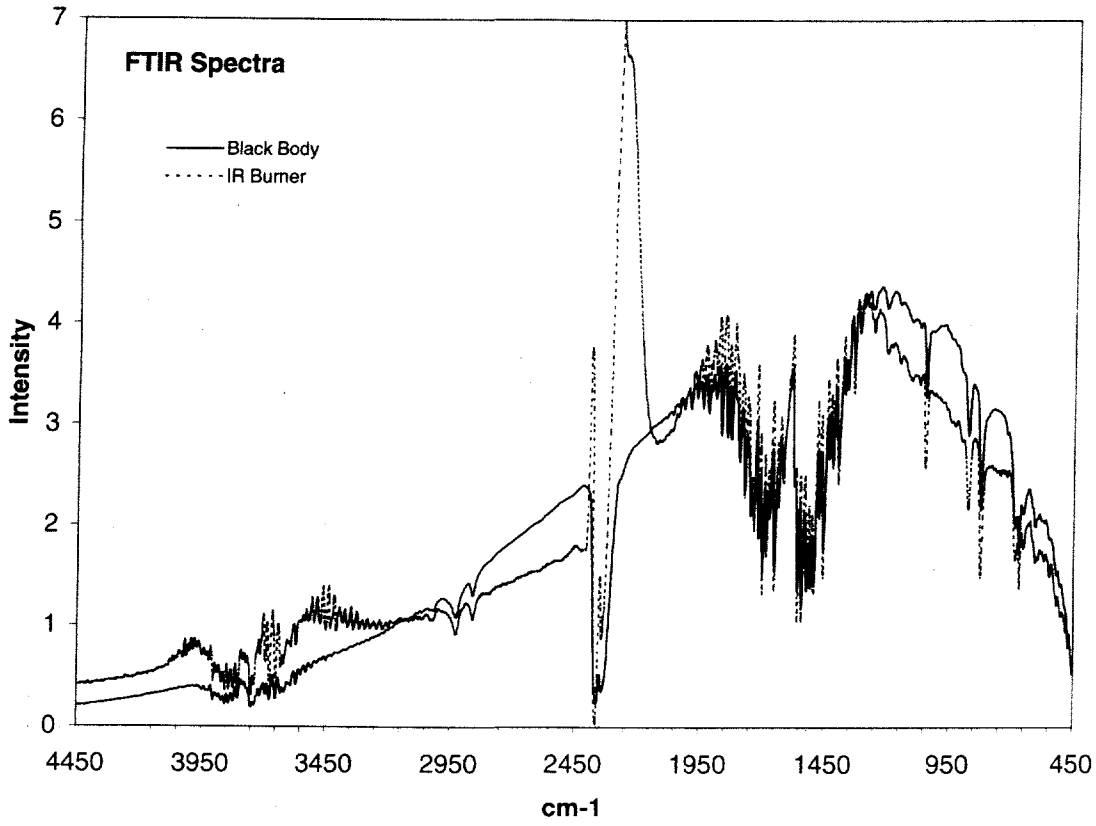

Fig. 6 FTIR spectra of the infrared burner and the black body.

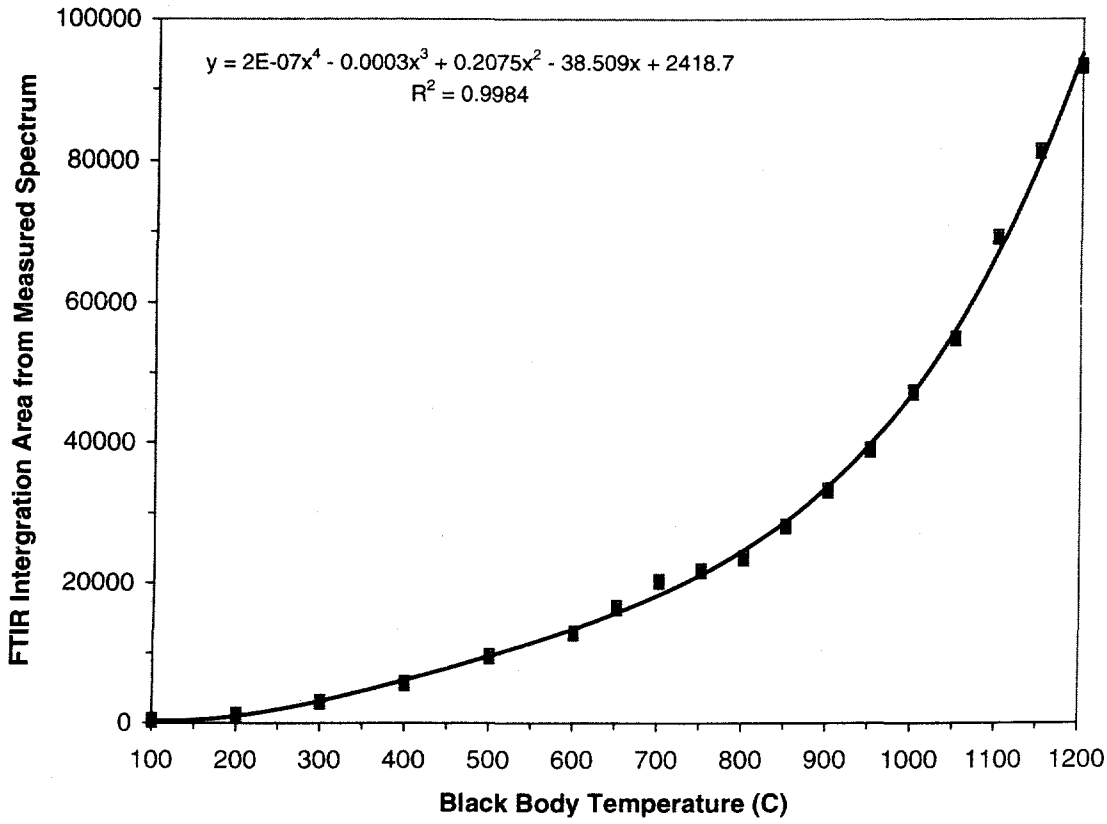

Fig. 7 Relationship between the measured FTIR integration area (6500 - 450 cm^{-1}) and the blackbody temperature (°C).

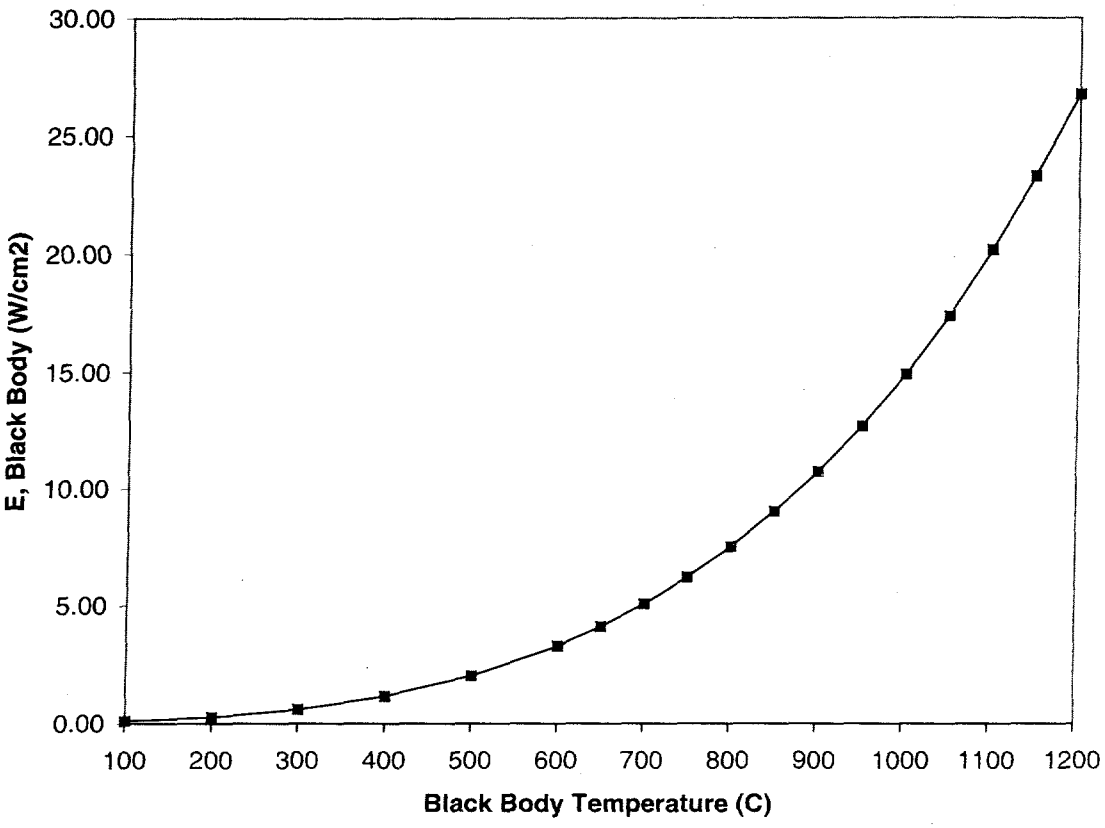

Fig. 8 Relationship between the total radiant energy ($E_b(T)$) calculated from the Stefan-Boltzmann law and the blackbody temperature (°C).

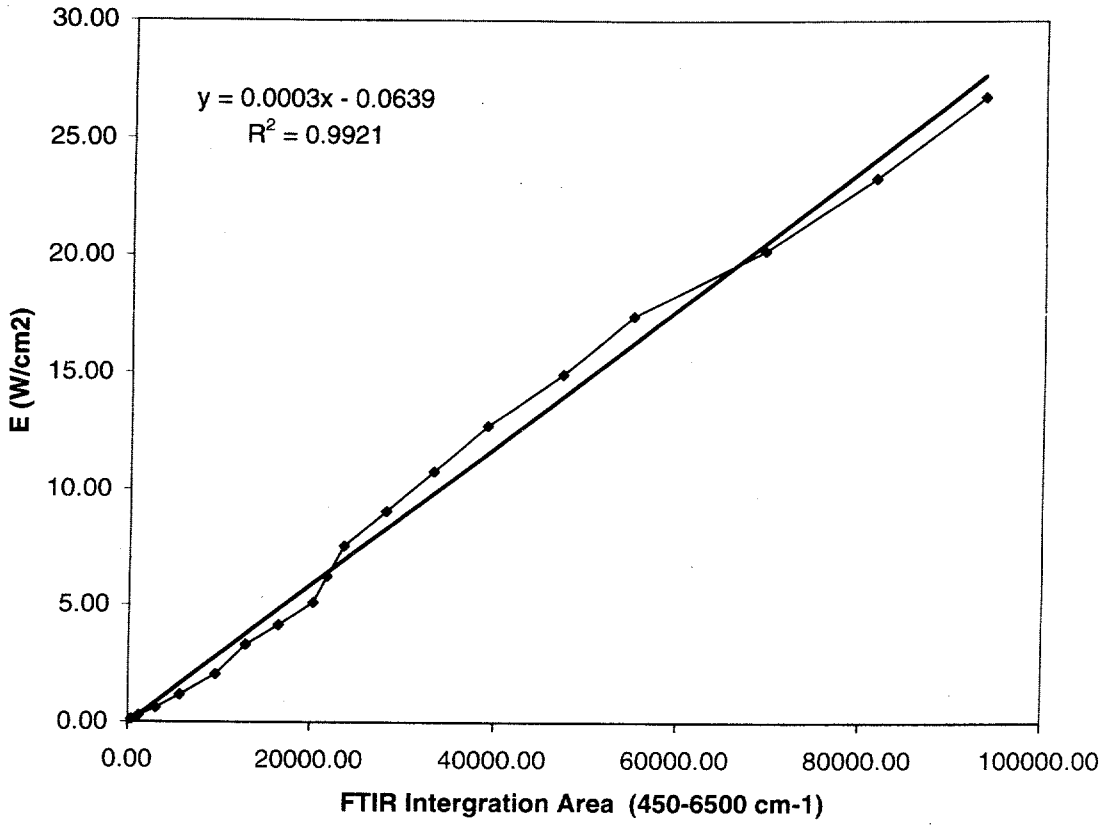

Fig. 9 Relationship between the total radiant energy ($E_b(T)$) calculated from the Stefan-Boltzmann law and the measured FTIR integration area (6500 - 450 cm^{-1}).

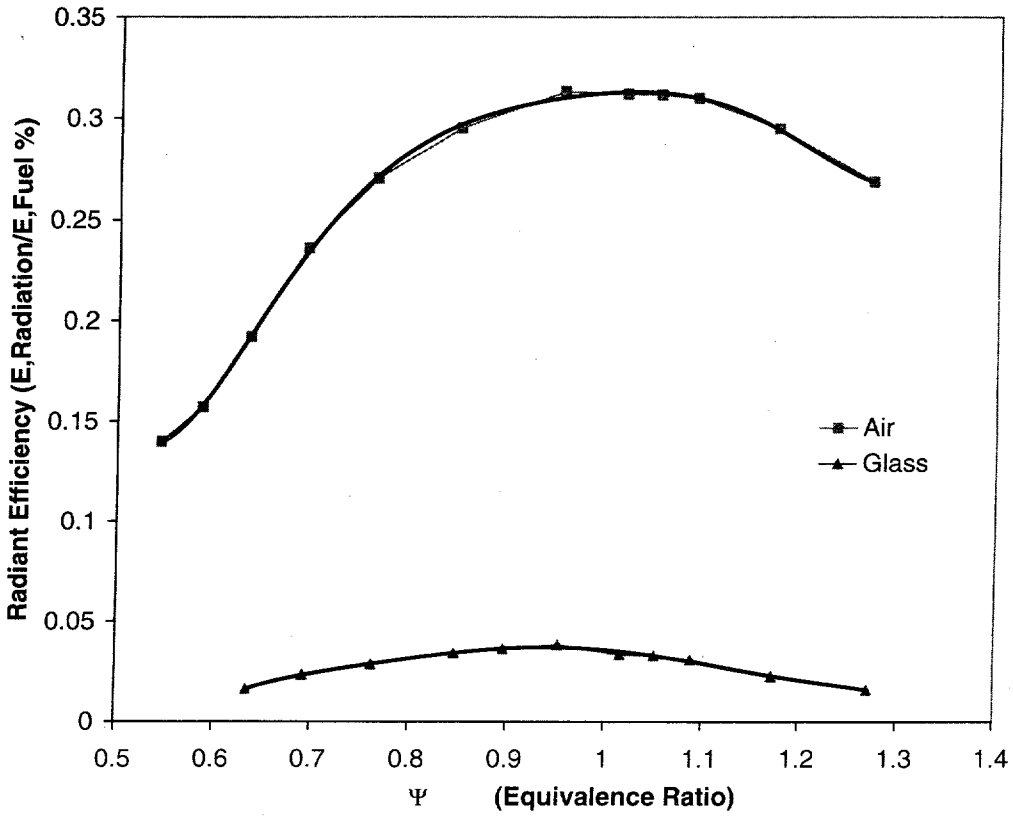

Fig. 10 Relationship of the radiant efficiency (the measured radiant energy / the total input fuel energy) and the equivalence ratio (the actual fuel-air ratio / the theoretical fuel-air ratio) for the methane-air combustion.

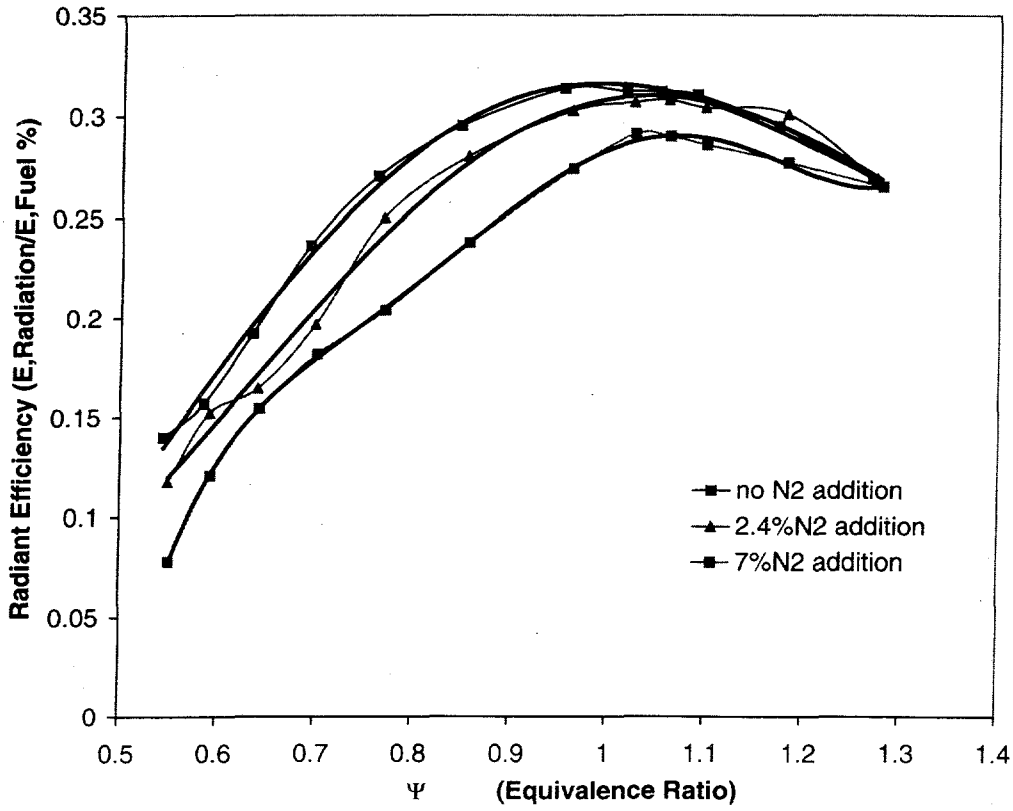

Fig. 11 Effects of the N_2 addition on the radiant efficiency.

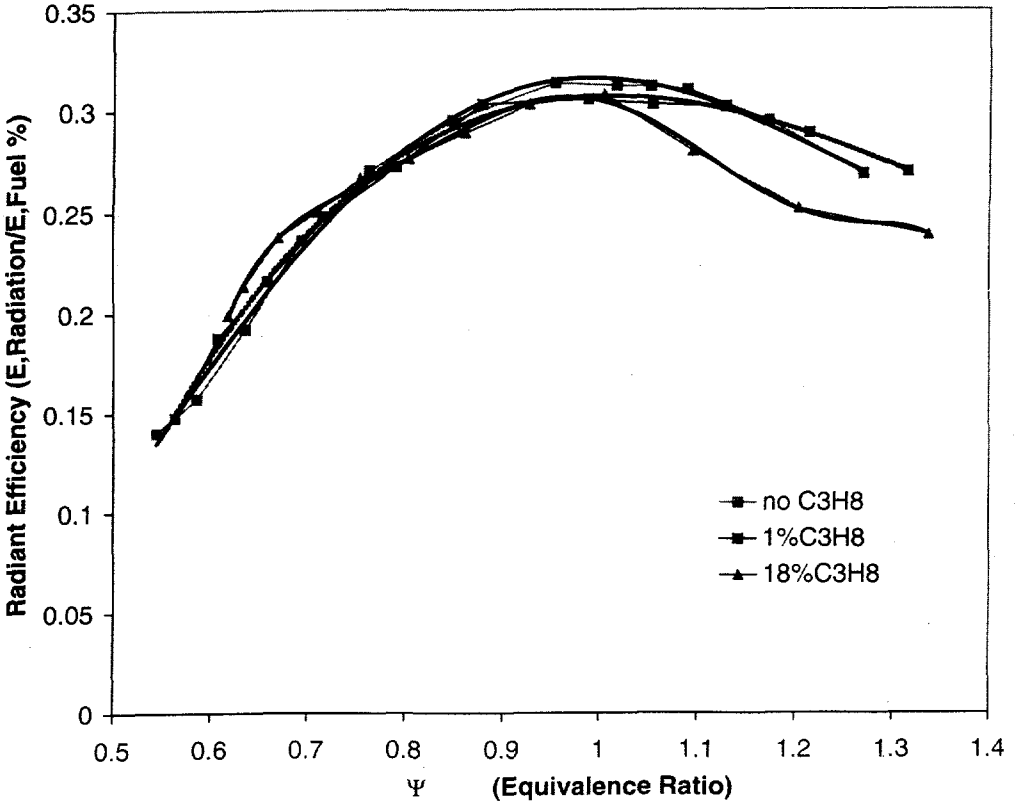

Fig. 12 Effects of the propane (C_3H_8) addition on the radiant efficiency.

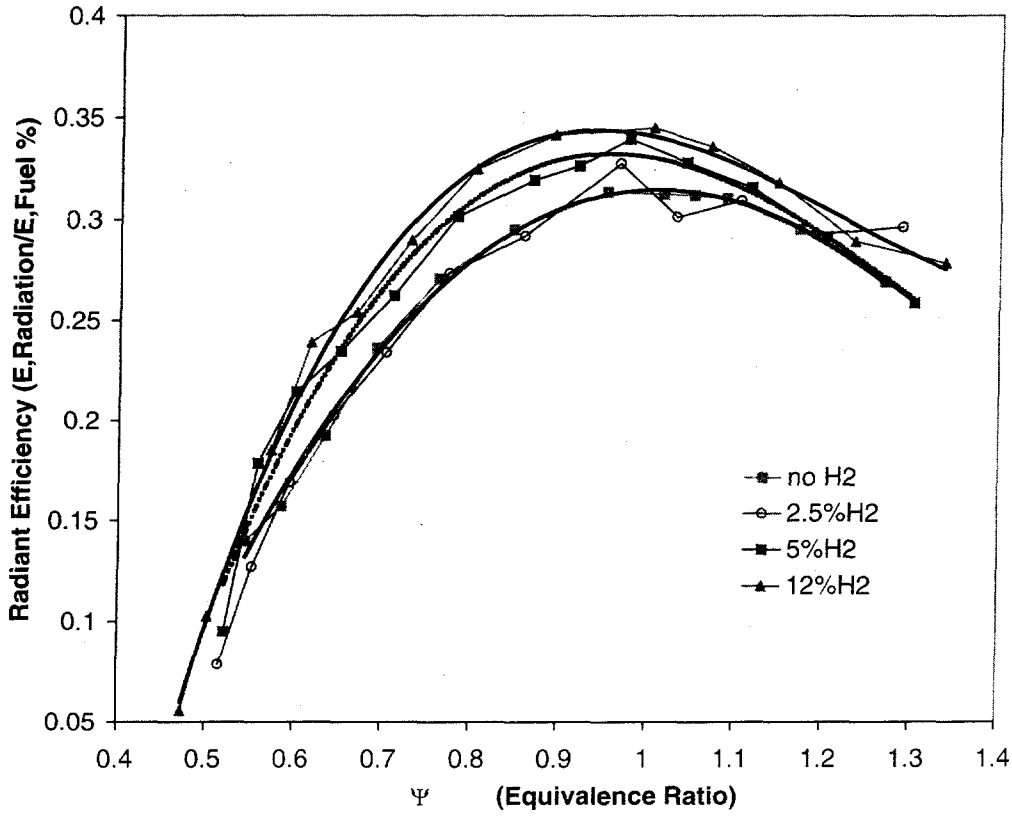

Fig. 13 Effects of the H_2 addition on the radiant efficiency.

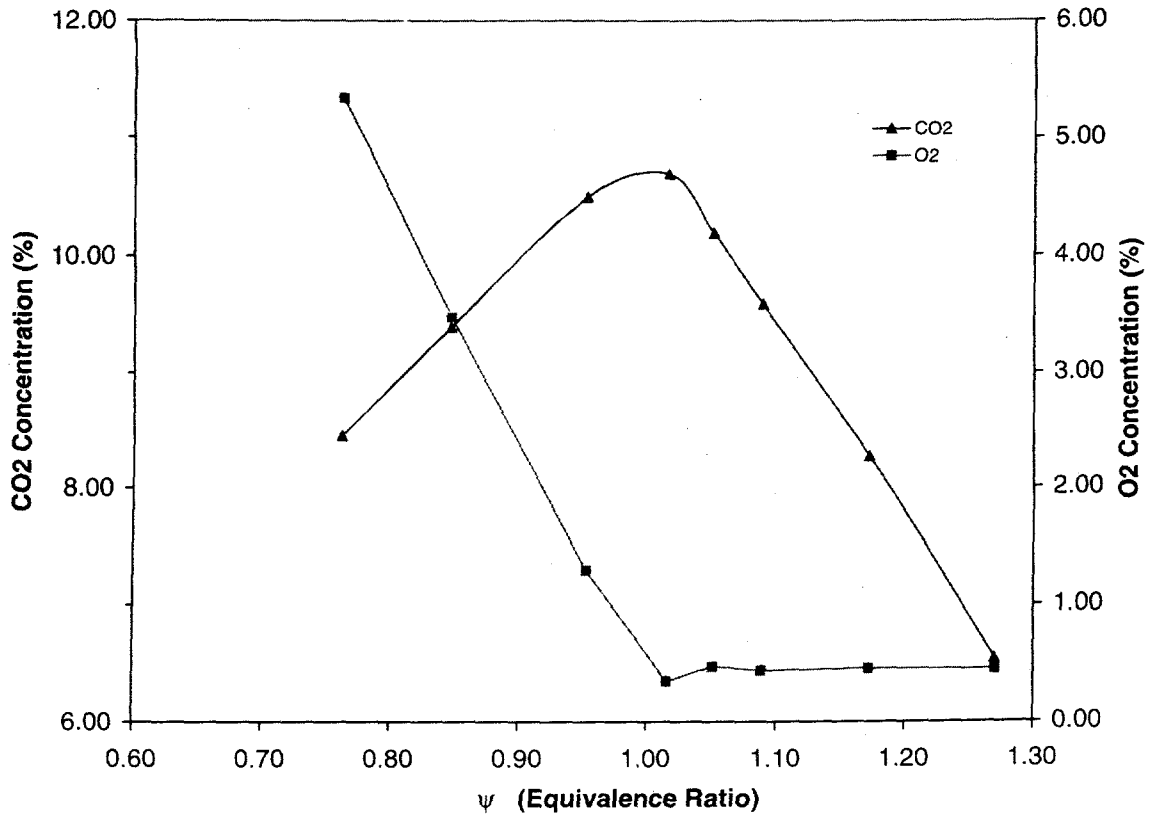

Fig. 14 CO_2 and O_2 concentrations in the combustion emission gas for the different equivalence ratio (methane + air).

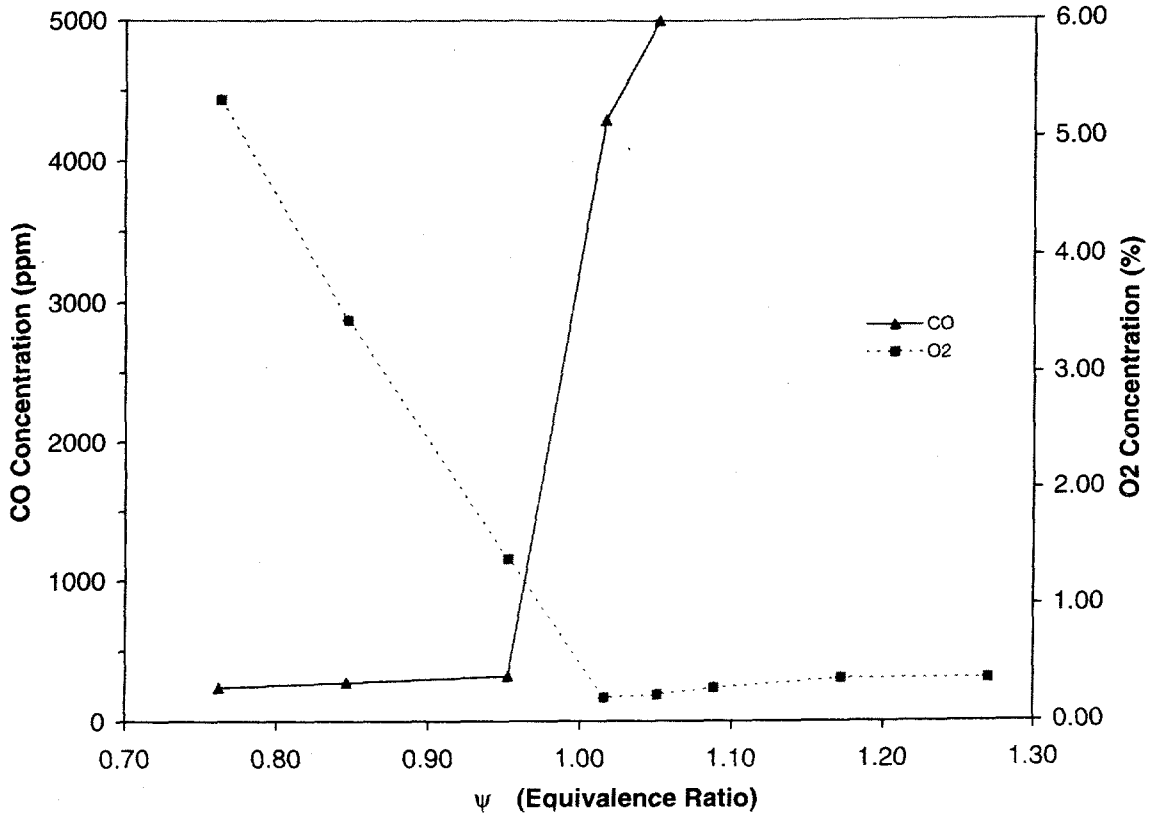

Fig. 15 CO and O_2 concentrations in tne combustion emission gas for the different equivalence ratio (methane + air).

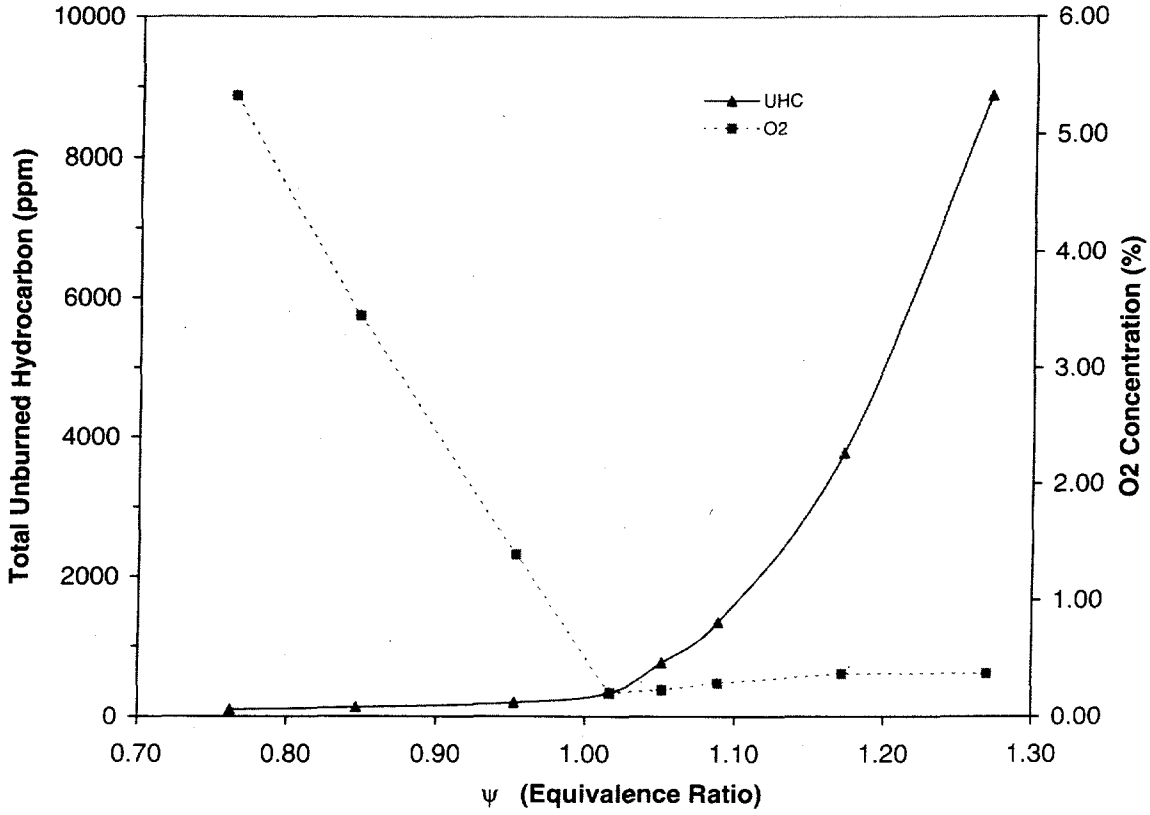

Fig. 16 Total unburned hydrocarbon (UHC) and O_2 concentrations in the combustion emission gas for the different equivalence ratio (methane + air).

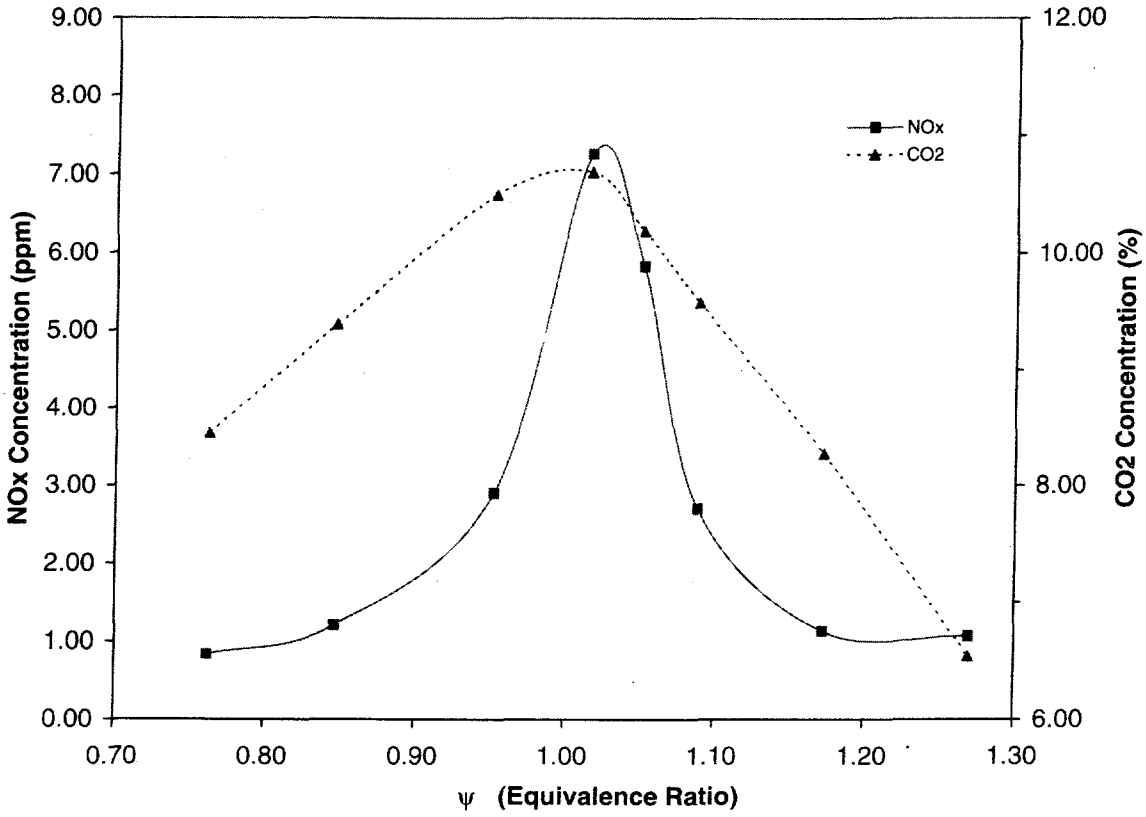

Fig. 17 NO_x and CO_2 concentrations in the combustion emission gas for the different equivalence ratio (methane + air).

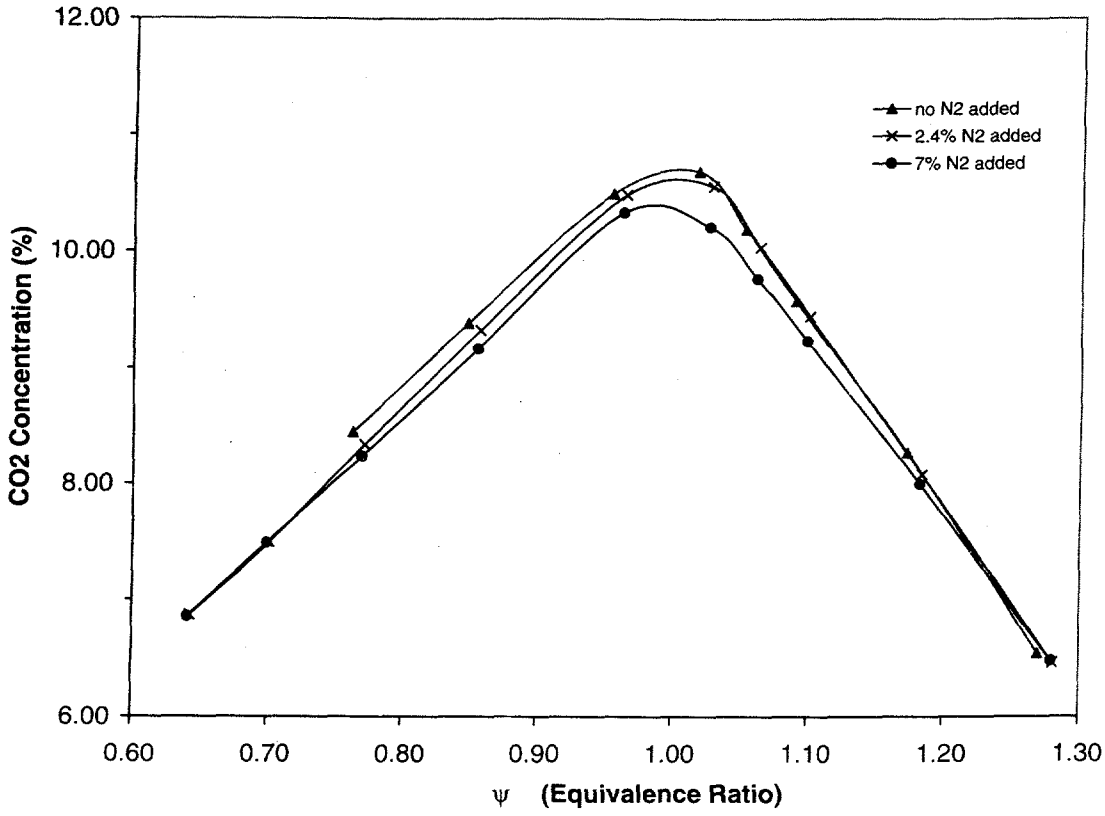

Fig. 18 Effect of the N_2 addition on the CO_2 concentration in the combustion emission gas.

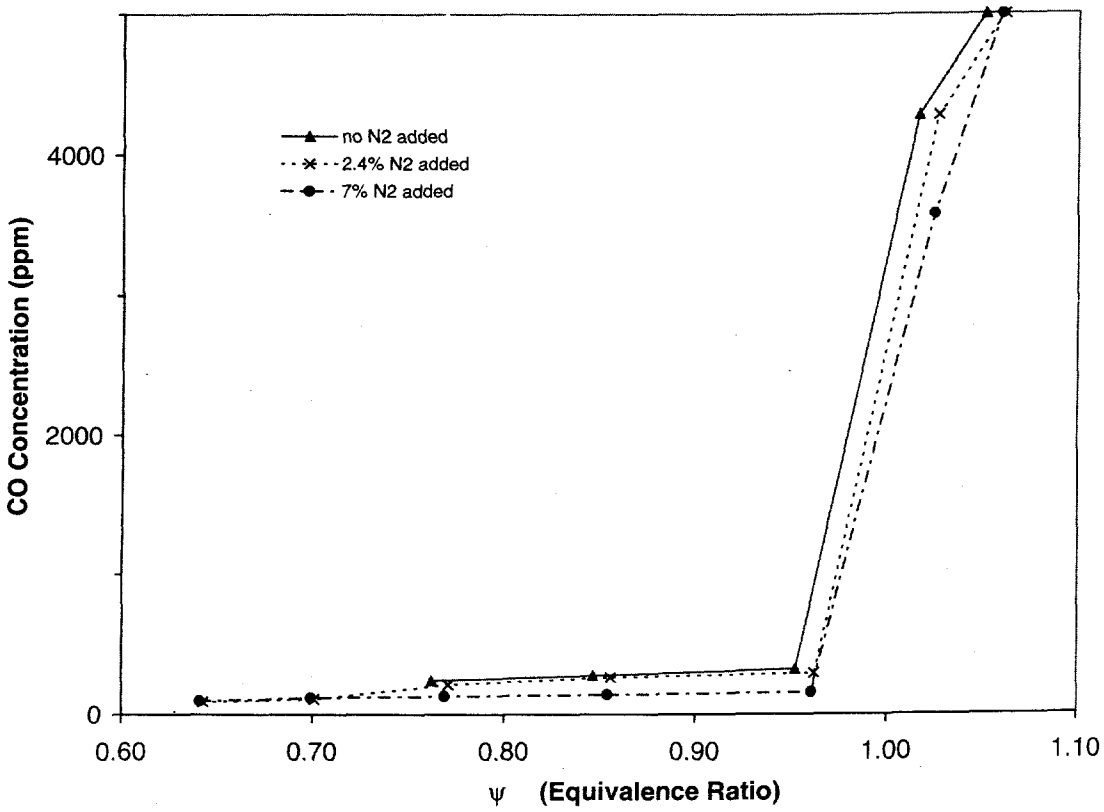

Fig. 19 Effect of the N_2 addition on the CO concentration in the combustion emission gas.

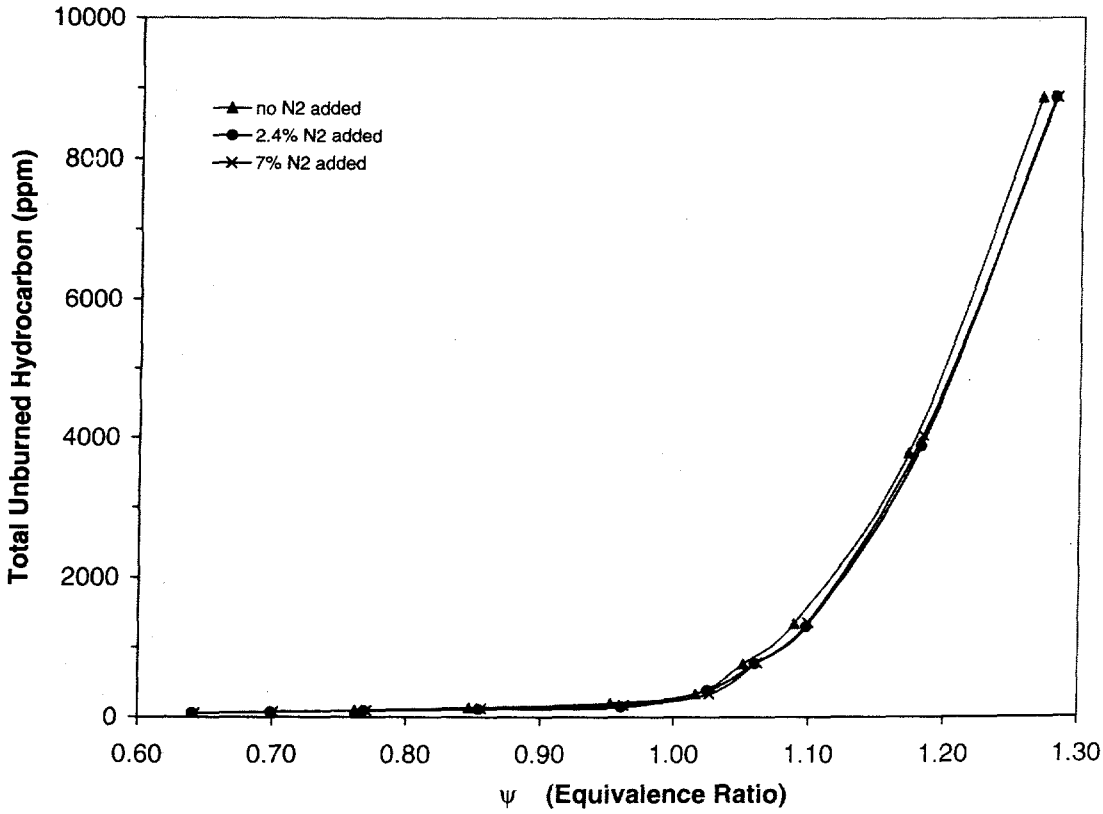

Fig. 20 Effect of the N_2 addition on the total-unburned-hydrocarbon concentration in the combustion emission gas.

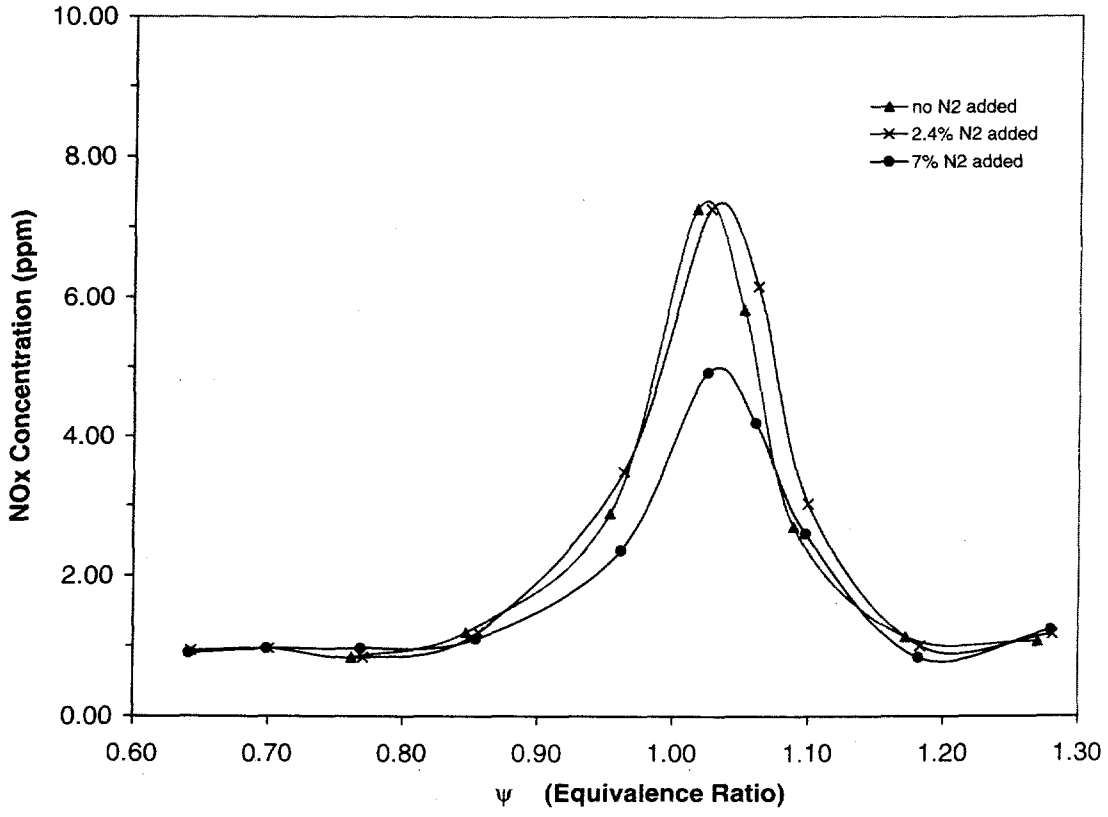

Fig. 21 Effect of the N_2 addition on the NOx concentration in the combustion emission gas.

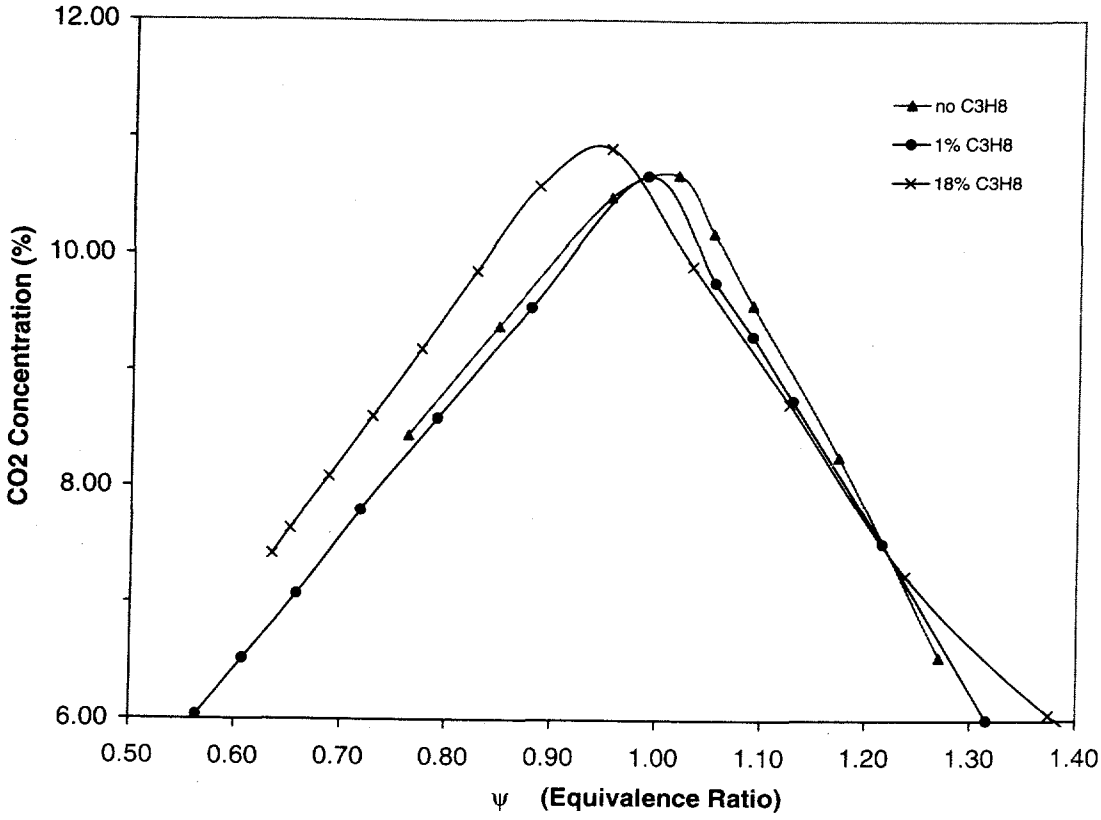

Fig. 22 Effect of the propane addition on the CO_2 concentration in the combustion emission gas.

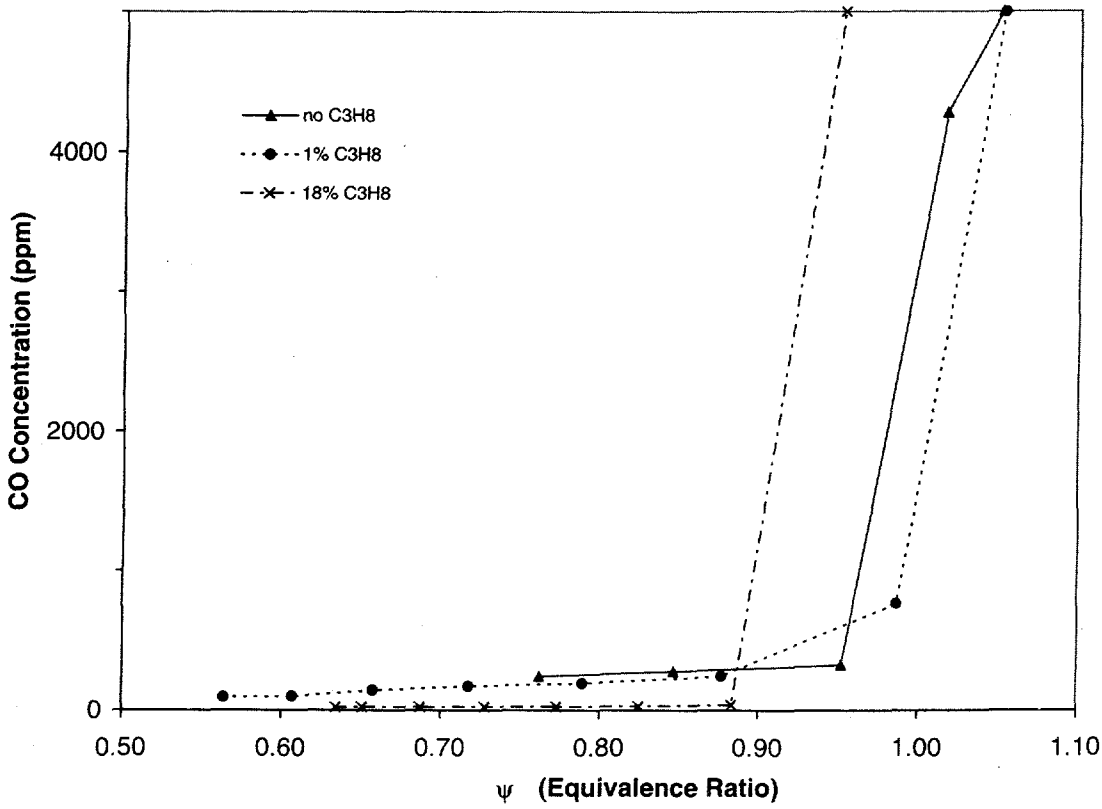

Fig. 23 Effect of the propane addition on the CO concentration in the combustion emission gas.

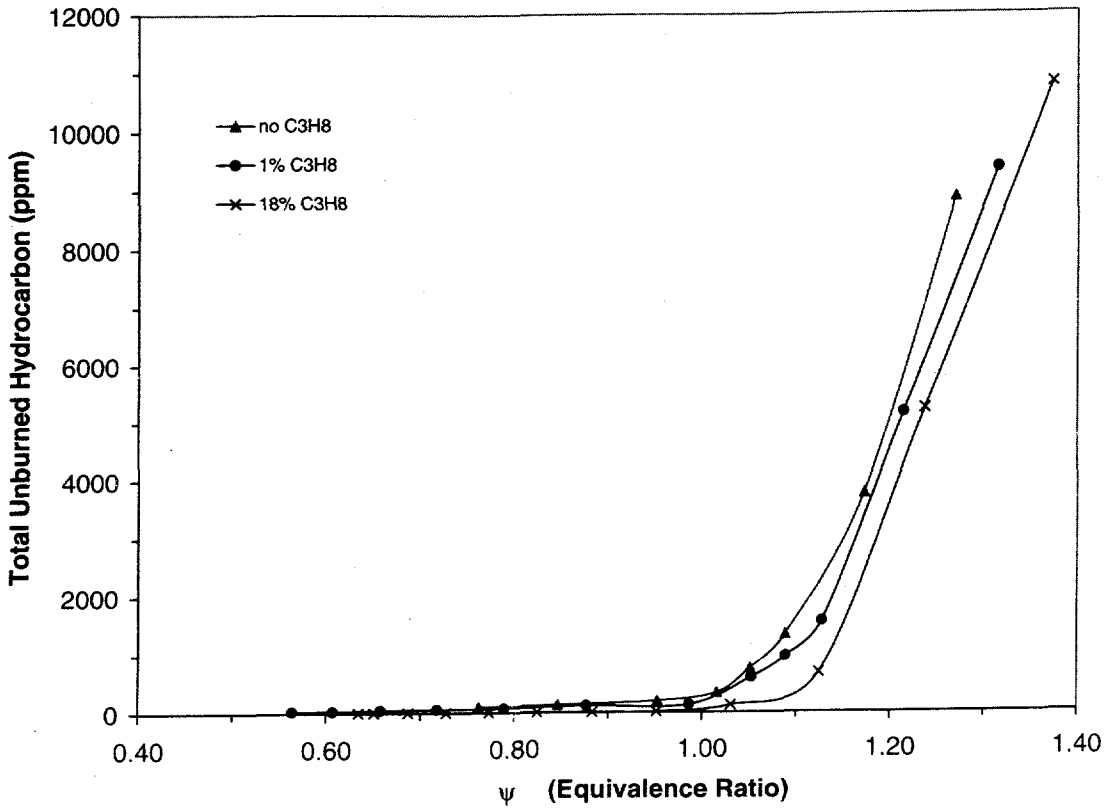

Fig. 24 Effect of the propane addition on the total-unburned-hydrocarbon concentration in the combustion emission gas.

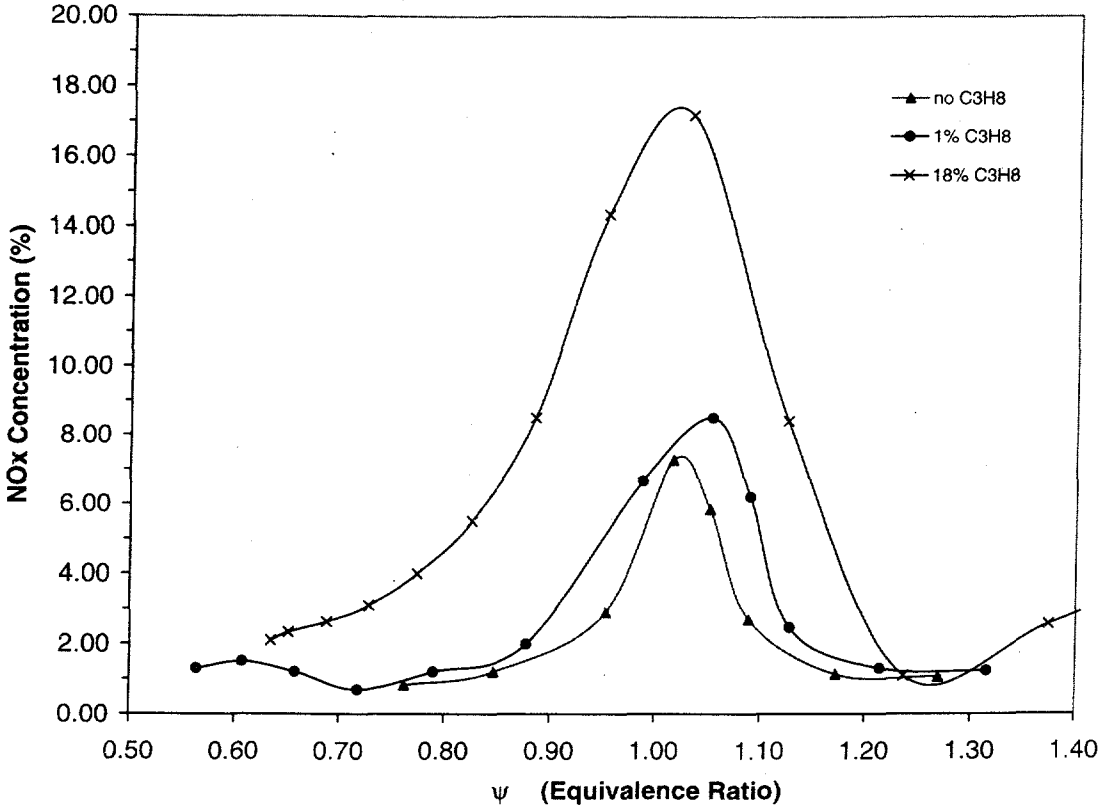

Fig. 25 Effect of the propane addition on the NOx concentration in the combustion emission gas.

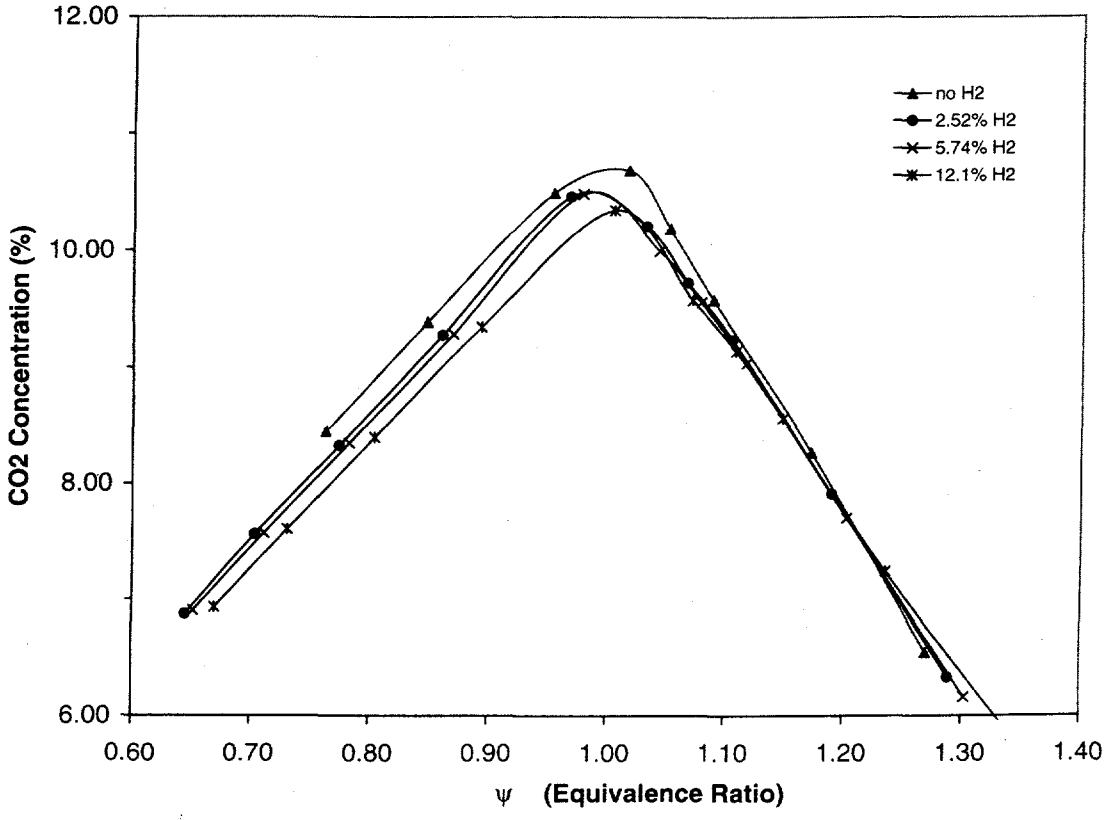

Fig. 26 Effect of the H_2 addition on the CO_2 concentration in the combustion emission gas.

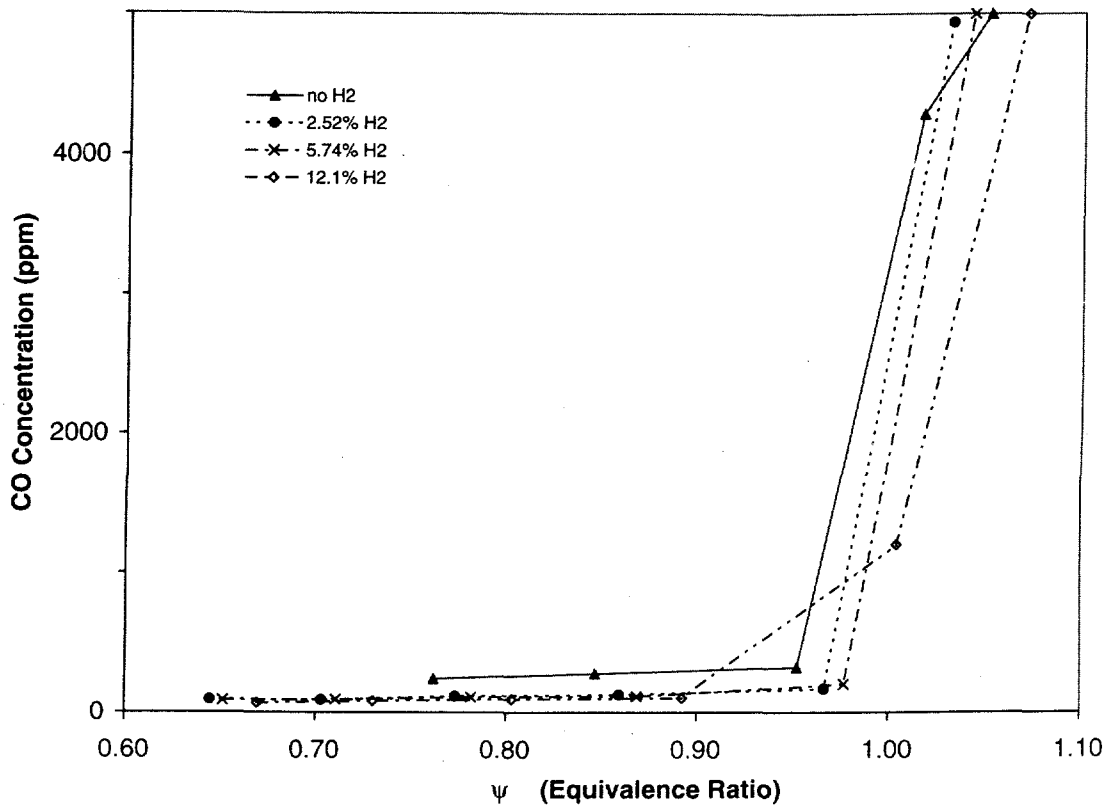

Fig. 27 Effect of the H_2 addition on the CO concentration in the combustion emission gas.

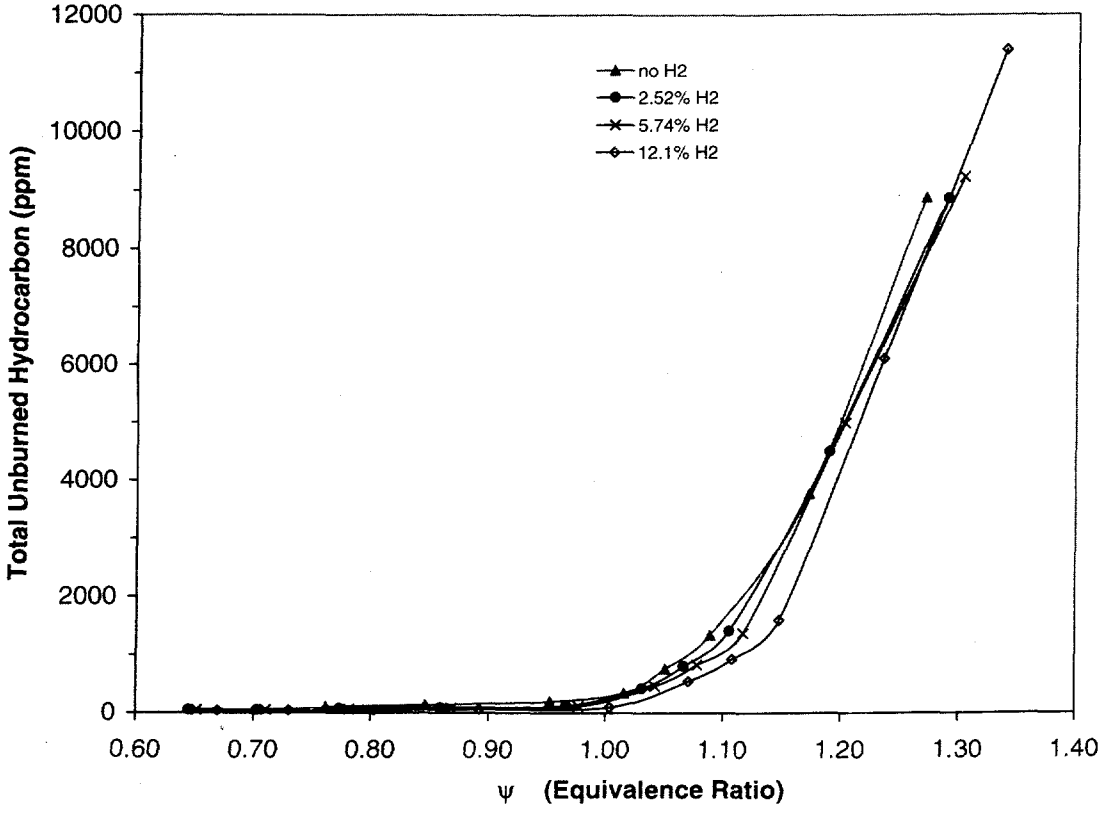

Fig. 28 Effect of the H_2 addition on the total unburned hydrocarbon concentration in the combustion emission gas.

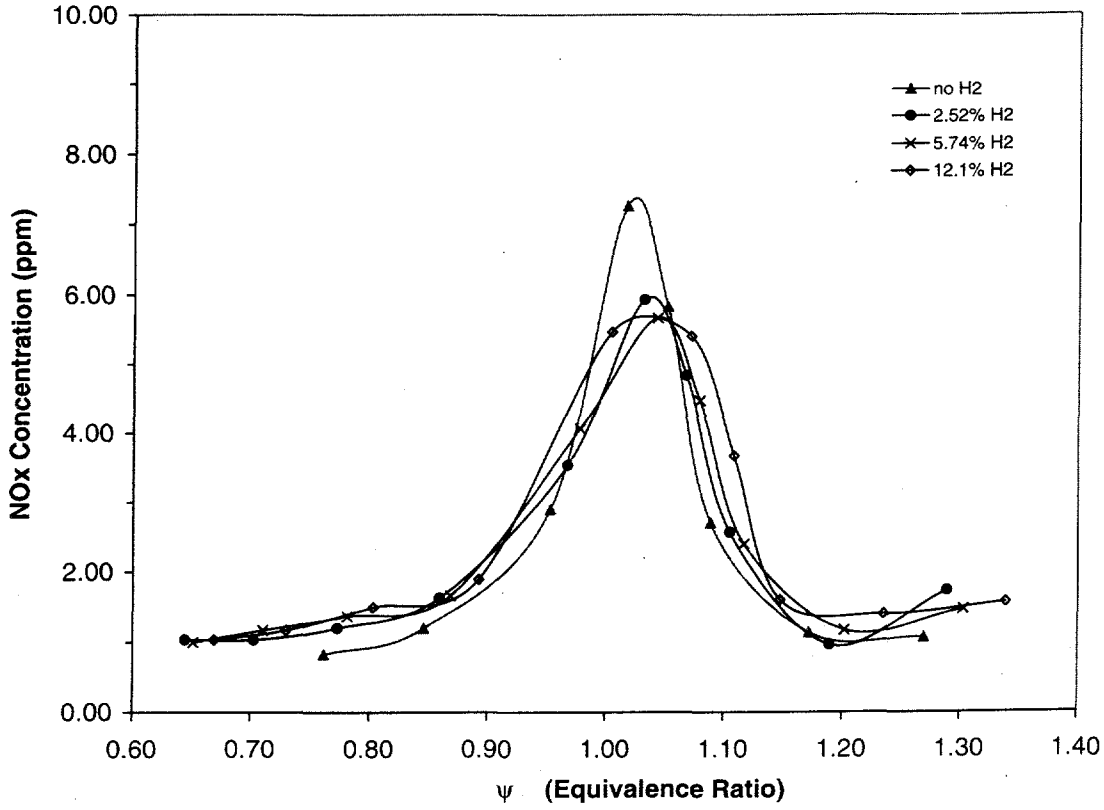

Fig. 29 Effect of the H_2 addition on the NOx concentration in the combustion emission gas.